

Article

Discovery of pteridin-7(8*H*)-one-based Irreversible Inhibitors targeting Epidermal Growth Factor Receptor (EGFR) Kinase T790M/L858R mutant

Wei Zhou, Xiaofeng Liu, Zhengchao Tu, Lianwen Zhang, Xin Ku,
Fang Bai, zhenjiang zhao, Yufang Xu, Ke Ding, and Honglin Li

J. Med. Chem., **Just Accepted Manuscript** • DOI: 10.1021/jm401045n • Publication Date (Web): 22 Sep 2013

Downloaded from <http://pubs.acs.org> on September 23, 2013

Just Accepted

"Just Accepted" manuscripts have been peer-reviewed and accepted for publication. They are posted online prior to technical editing, formatting for publication and author proofing. The American Chemical Society provides "Just Accepted" as a free service to the research community to expedite the dissemination of scientific material as soon as possible after acceptance. "Just Accepted" manuscripts appear in full in PDF format accompanied by an HTML abstract. "Just Accepted" manuscripts have been fully peer reviewed, but should not be considered the official version of record. They are accessible to all readers and citable by the Digital Object Identifier (DOI®). "Just Accepted" is an optional service offered to authors. Therefore, the "Just Accepted" Web site may not include all articles that will be published in the journal. After a manuscript is technically edited and formatted, it will be removed from the "Just Accepted" Web site and published as an ASAP article. Note that technical editing may introduce minor changes to the manuscript text and/or graphics which could affect content, and all legal disclaimers and ethical guidelines that apply to the journal pertain. ACS cannot be held responsible for errors or consequences arising from the use of information contained in these "Just Accepted" manuscripts.



ACS Publications
High quality. High impact.

Journal of Medicinal Chemistry is published by the American Chemical Society, 1155 Sixteenth Street N.W., Washington, DC 20036
Published by American Chemical Society. Copyright © American Chemical Society. However, no copyright claim is made to original U.S. Government works, or works produced by employees of any Commonwealth realm Crown government in the course of their duties.

Discovery of pteridin-7(8*H*)-one-based Irreversible Inhibitors targeting Epidermal Growth Factor Receptor (EGFR) Kinase T790M/L858R mutant

*Wei Zhou^{†,‡}, Xiaofeng Liu^{†,‡}, Zhengchao Tu^{¶,‡}, Lianwen Zhang[¶], Xin Ku^{||}, Fang Bai^{§, #}, Zhenjiang Zhao[†], Yufang Xu^{†, *}, Ke Ding^{¶, *}, Honglin Li^{†, *}*

[†]Shanghai Key Laboratory of New Drug Design, State Key Laboratory of Bioreactor Engineering, School of Pharmacy, East China University of Science & Technology, Shanghai 200237, China. [¶]Key Laboratory of Regenerative Biology and Institute of Chemical Biology, Guangzhou Institutes of Biomedicine and Health, Chinese Academy of Sciences, Guangzhou 510530, China. ^{||}Lehrstuhl für Proteomik und Bioanalytik, Technische Universität München, 85354 Freising, Germany. [§]Faculty of Chemical, Environmental and Biological Science and Technology, [#]Department of Engineering Mechanics, State Key Laboratory of Structural Analysis for Industrial Equipment, Dalian University of Technology, Dalian 116023, China.

[‡] Authors contributed equally to this work

* To whom correspondence should be addressed. hlli@ecust.edu.cn, yfxu@ecust.edu.cn, ding_ke@gibh.ac.cn

Please address correspondence and requests for reprints to:

1
2
3 Prof. Honglin Li
4

5
6 School of Pharmacy, East China University of Science and Technology
7

8
9
10 130 Mei Long Road, Shanghai 200237
11

12
13 Phone/Fax: +86-21-64250213
14

15
16 Email: hlli@ecust.edu.cn
17
18
19
20
21
22
23
24
25
26
27
28
29
30
31
32
33
34
35
36
37
38
39
40
41
42
43
44
45
46
47
48
49
50
51
52
53
54
55
56
57
58
59
60

ABSTRACT: The EGFR T790M variant is an important mutation resulting in approximately 50% of the clinically acquired resistance to approved EGFR inhibitors. Starting with previously reported pyrimidine-based EGFR inhibitor, a novel pteridin-7(8*H*)-one scaffold with high 3D similarity was found and transformed into irreversible inhibitors of EGFR T790M mutant. The most potent compounds, **3q** and **3x**, exhibited excellent enzyme inhibitory activities with subnanomolar IC₅₀ values for both wild-type and double T790M/L858R mutant of EGFRs, as well as potent cellular antiproliferative activities against both gefitinib-sensitive and -resistant cancer cell lines. *In vivo* antitumor efficacy study demonstrated that compound **3x** significantly inhibited the tumor growth and induced tumor stasis in an EGFR-T790M/L858R driven human NSCLC xenograft mouse model. This work demonstrated the utility of this sophisticated computational design strategy for fast 3D scaffold hopping with competitive bioactivities to meet an important clinical need.

Keywords: 3D molecular similarity, Scaffold hopping, Epidermal growth factor receptor; Irreversible inhibitors

Abbreviations: EGFR, epidermal growth factor receptor; SHAFTS, SHApe-FeaTure Similarity; NCI, National Cancer Institute; NSCLC, non-small-cell lung cancer; WT, wild-type; PDB, Protein Data Bank; SAR, structure–activity relationship; JAK3, Janus kinase 3; BLK, B lymphocyte kinase; FLT3, FMS-like tyrosine kinase 3; HER2, human epidermal growth factor receptor 2; TLC, thin-layer chromatography; HPLC, high-performance liquid chromatography; DIPEA, N,N-diisopropylethylamine; intraperitoneal, IP.

INTRODUCTION

The epidermal growth factor receptor (EGFR) tyrosine kinase plays a crucial role in cell signal transduction pathways and is closely related to cell proliferation, survival, adhesion, migration, and differentiation.¹⁻² Thus, EGFR tyrosine kinase has become an attractive therapeutic target for cancer treatment, especially non-small-cell lung cancer (NSCLC) treatment.³⁻⁵ Gefitinib (Iressa) and Erlotinib (Tarceva), which reversibly inhibit the EGFR tyrosine kinase,¹ are approved for the treatment of NSCLC. Gefitinib and erlotinib are effective inhibitors of the wild-type (WT) EGFR and some drug-sensitive mutants (such as L858R and delE746_A750) associated with NSCLC.⁶⁻⁸ However, their clinical efficacies are limited by acquired point mutations and the upregulation of bypass signaling pathways.⁹⁻¹⁰ The substitution of the gatekeeper residue threonine 790 with methionine (T790M mutation) in the catalytic domain of the EGFR was detected in approximately 50% of the NSCLC patients with acquired resistance after treatment with gefitinib or erlotinib.¹¹⁻¹³ The T790M mutation of EGFR has a modest affinity for gefitinib or erlotinib binding; however, this mutation increases the binding affinity for ATP. This change in relative affinity is the primary mechanism by which the T790M mutation confers drug resistance.¹⁴⁻¹⁵ Several irreversible EGFR tyrosine kinase inhibitors (such as CI-1033,¹⁶ EKB-569,¹⁷ BIBW2992,¹⁸ HKI-272,¹⁹ and PF00299804²⁰) have been developed to overcome resistance caused by the T790M mutation. These irreversible inhibitors contain an electrophilic Michael addition receptor moiety which can covalently alkylate the conserved cysteine residue (Cys797) close to the ATP binding site of the EGFR.²¹⁻²² The formation of the covalent bond allows these irreversible inhibitors to achieve greater occupancy of the ATP site and higher selectivity for the EGFR-family tyrosine kinases relative to the reversible inhibitors.^{11, 23-24} However, only a few of the current irreversible inhibitors show promising safety and efficacy results in clinic trials.²⁵⁻²⁶

Therefore, the discovery of novel irreversible inhibitors with alternative scaffolds that are effective against wild-type and T790M-mutated EGFRs is of great importance.

In our previous studies, a pyrimidine core compound **1** (Figure 1) was identified as a reversible inhibitor with moderate affinity of wild-type ($IC_{50} = 7.7 \mu M$) and T790M-mutated EGFRs ($IC_{50} = 36.1 \mu M$) through a receptor-based and ligand-based combined virtual screening protocol.²⁷ Based on the results of the docking simulation, this compound could likely be converted into a potent and irreversible inhibitor of the EGFR T790M mutant by introducing a Michael addition receptor at the benzene ring **A**. However, a pyrimidine scaffold-based irreversible inhibitor of the T790M mutant has been already reported and patented.^{15,28} One of the most active and selective inhibitors, WZ4002 (**1a**), inhibited the proliferation of the cancer cells or Ba/F3 cells expressing the L858R, delE746-A750, and/or T790M-mutated EGFR more potently than those expressing the wild-type EGFR cells.¹⁵ Replacing the pyrimidine with biologically related chemotypes (scaffold hopping) to design a novel T790M mutant-specific inhibitor provides a desirable approach for discovering novel compounds with competitive bioactivities, while avoiding the intellectual property (IP) issues with the compound WZ4002.

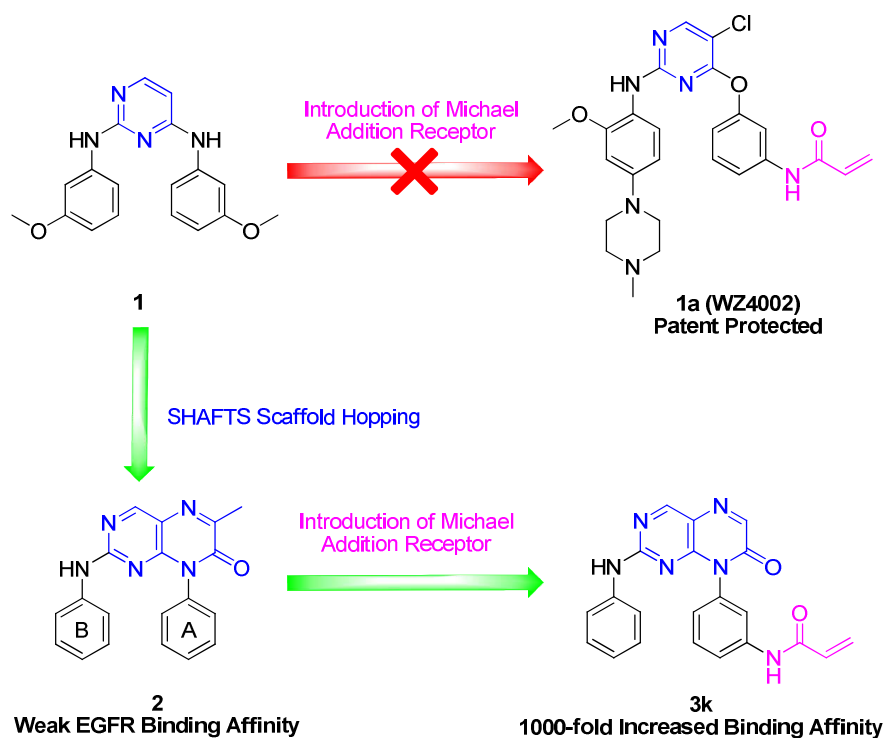


Figure 1. Discovery of novel pteridin-7(8H)-one EGFR T790M mutant inhibitors by computational scaffold hopping.

There are many routine and specifically designed computational methods to perform scaffold hopping, including pharmacophore matching,²⁹⁻³¹ molecular similarity,³²⁻³⁴ molecular superposition,³⁵⁻³⁷ and moiety replacement,³⁷ however, most of these methods have only been evaluated in theory. We recently developed SHAFTS, a hybrid 3D similarity calculation method. The performance of this method in a retrospective virtual screening was reported in which known active compounds as well as corresponding chemotypes of decoys for multiple target sets were enriched.³⁸ As the proof-of-concept case for computational scaffold hopping with SHAFTS, the pyridine moiety in hit compound **1** was converted to a pteridin-7(8H)-one scaffold (**2**) by querying against the National Cancer Institute (NCI) compound database with SHAFTS. Compound **2** exhibited weak binding affinity against both the wild-type and T790M mutant EGFRs. Aspired by the design strategy of WZ4002, further decoration of **2** with Michael

1
2
3 addition receptors to mimic the irreversible binding mode of WZ4002 in T790M crystal structure
4
5 resulted in a series of high-potency inhibitors effective against both the wide-type and T790M
6
7
8 mutant EGFRs. These irreversible EGFR inhibitors exhibited similar binding modes and potent
9
10 inhibitory activities against the EGFRs similar to those of WZ4002 but with completely novel
11
12 scaffold, indicating that molecular 3D similarity can be remarkably helpful in scaffold hopping
13
14
15 with a carefully conceived design strategy.
16
17
18
19
20
21
22
23
24
25
26
27
28
29
30
31
32
33
34
35
36
37
38
39
40
41
42
43
44
45
46
47
48
49
50
51
52
53
54
55
56
57
58
59
60

RESULTS AND DISCUSSION

The Discovery of Novel Irreversible EGFR Inhibitors through Computational Scaffold Hopping. In our previous study, compound **1** via virtual screening was identified as a moderately effective EGFR kinase inhibitor, which shares the same pyrimidine scaffold as the recently developed irreversible EGFR T790M mutant inhibitor WZ4002. Therefore, a similar strategy could likely be applied to convert compound **1** into a potential EGFR mutant inhibitor by introducing a Michael addition receptor group. However, because WZ4002-based irreversible inhibitors have been previously reported and patented, the pyridine scaffold had to be replaced with a different scaffold prior to Michael addition receptor decoration that could bind the EGFR pocket in a similar manner. Shape based molecular 3D superposition proved a powerful tool for computational scaffold hopping because shape complementation plays a pivotal role in ligand-protein recognition.³⁹ We have developed an in-house molecular 3D similarity calculation method called SHAFTS, SHAFTS adopts hybrid similarity metric combined with molecular shape and colored (labeled) chemistry groups annotated by pharmacophore features for 3D similarity calculation and ranking, which is designed to integrate the strength of pharmacophore matching and volumetric overlay approaches. A feature triplet hashing method is used for fast molecular alignment poses enumeration, and the optimal superposition between the target and the query molecules can be prioritized by calculating corresponding “hybrid similarities”. SHAFTS is suitable for large-scale virtual screening with single or multiple bioactive compounds as the query “templates” regardless of whether corresponding experimentally determined conformations are available.³⁸ By superimposing the shapes of the optimized candidate compounds and key chemotype characteristics onto the query template, novel bioactive compounds can be identified with similar shapes and modes of binding, but different

2D topological structures. In our previous study, SHAFTS outperformed several other widely used virtual screening methods in terms of enrichment of known active compounds as well as novel chemotypes. As a benchmark of prospective virtual screening, SHAFTS was applied to successfully identify novel RSK2 kinase inhibitors with sub-micromolar inhibitory activities,⁴⁰ thereby demonstrating its robustness in hit compounds identification and the potential of scaffold hopping in virtual screening.

To identify novel scaffold for EGFR irreversible inhibitor design, Open National Cancer Institute (NCI) database (Release 3, September 2003) containing approximately 250K compounds was searched, which represents the publicly available part of the over half-million structures collection assembled by the NCI in the course of a more than 50 years' long effort of screening compounds against cancer. The NCI database used was proved to hold the highest number of compounds that are unique to it because approximately 200 000 of the NCI structures were not found in most of the other analyzed databases.⁴¹ Both SHAFTS and NCI database were integrated into an online web server called ChemMapper for automatic searching for the most similar compounds in terms of 3D SHAFTS similarity metric.⁴² Using the truncated crystal structure of the EGFR with bound WZ4002 (without Michael receptor moiety) as the query, SHAFTS was applied to search the NCI compound database to discover novel compounds in which the pyrimidine core in compound **1** had been replaced, while preserving the two linked aromatic rings. The top-ranked molecules with SHAFTS similarities > 1.0 (maximum 2.0) were reserved. The two benzene rings attached on the pyrimidine scaffold are preferred to be reserved for introducing Michael addition receptor. According to these selection criteria, the pteridin-7(8*H*)-one based compound **2** (NSC86929) ranked highest in the hit list of hits, with a hybrid SHAFTS 3D similarity score of 1.44. The overlay poses between WZ4002 and NSC86929 in the

EGFR pocket calculated by SHAFTS are shown in Figure 2. The pteridin-7(8*H*)-one moiety overlays onto the pyridine ring well without obviously clashes with the binding pocket. This scaffold also supports the placement of the two linked benzene rings in the hydrophobic hotspots occupied by the same moieties on WZ4002. Moreover, the pteridin-7(8*H*)-one scaffold possesses the pivotal chemotype features that can form potential hydrogen bonds with the EGFR hinge region. Like those observed in the WZ4002 crystal structure, these structures occupy the position of the hydrophobic sub-pocket around the T790M mutant, indicating that NSC86929 binds to EGFR in the similar manner with the pyridine compounds. The NSC86929 has been tested using NCI anticancer assays involving multiple tumor cell strains, but was unfortunately found to be completely inactive.⁴³ However, encouraged by the high similarity of shape as well as key pharmacophore features between the pteridin-7(8*H*)-one and pyridine scaffolds, we believe the binding affinity of simple pteridin-7(8*H*)-one compound for EGFR can be increased by being converted into an irreversible EGFR inhibitor via Michael acceptor decoration, as we initially planned for compound **1**.

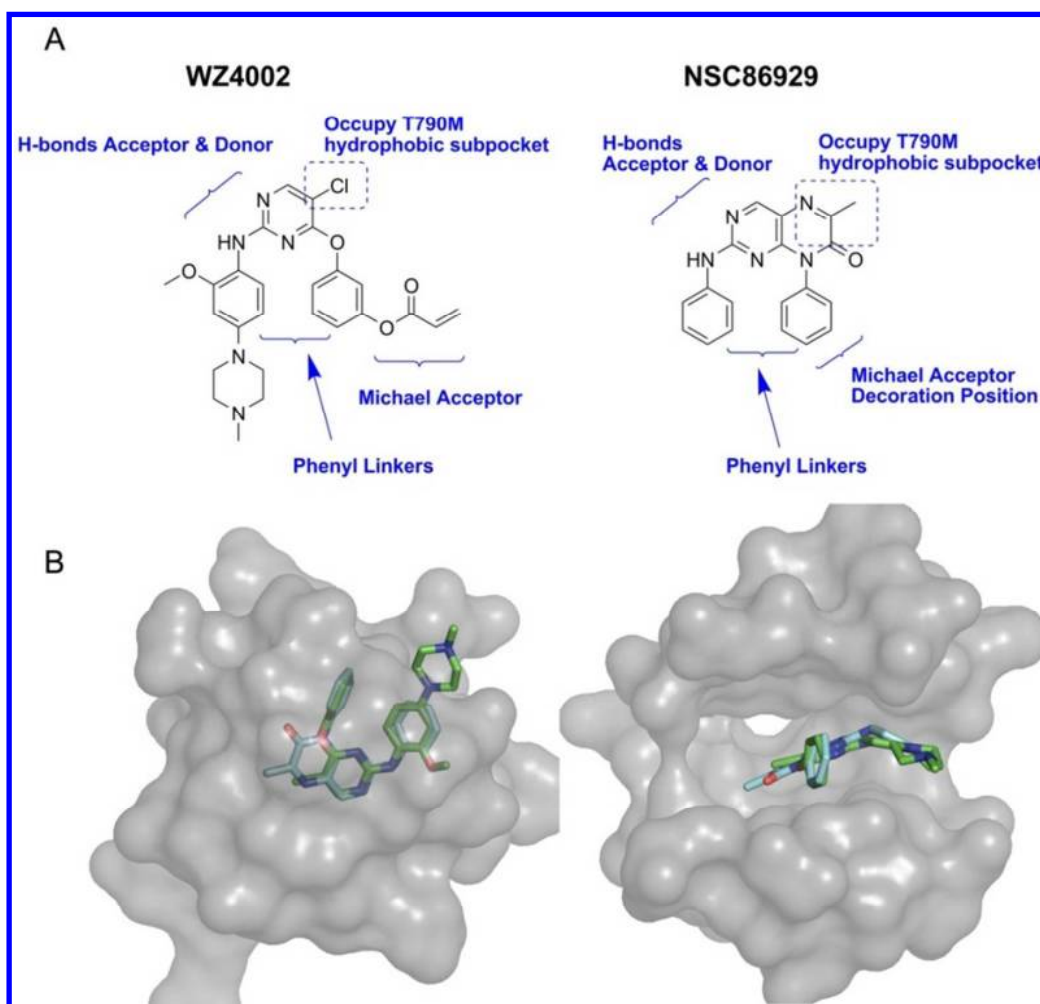
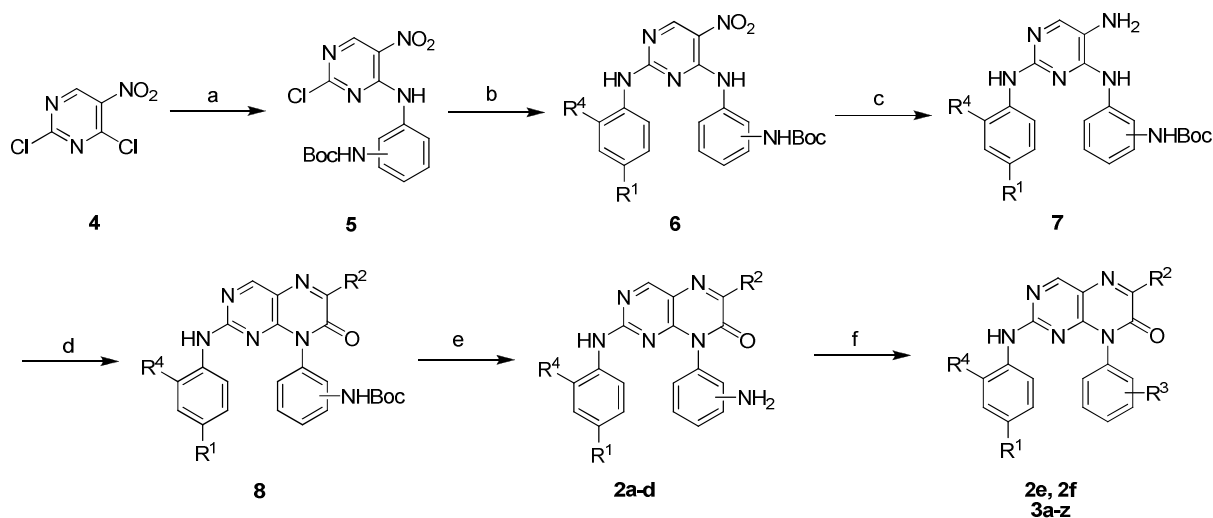


Figure 2. (A) The chemical structures of WZ4002 and NSC86929 are shown schematically in a manner highlighting all putative key interaction chemotype features in the complex with the kinase. (B) Overlay poses between WZ4002 (co-complexed crystal conformation, PDB code: 3IKA) and NSC86929 calculated by SHAFTS, with their carbons colored in green and cyan, respectively. The ATP-binding site of the EGFR T790M mutant is shown in the transparent molecular surface representation.

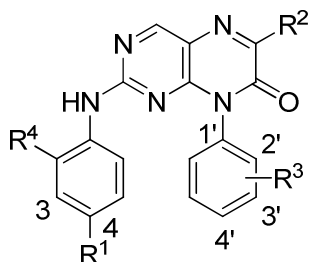
We first designed and synthesized four simple analogues of NSC86929 with the pteridin-7(8H)-one scaffold (**2a**, **2b**, **2c** and **2d**) (Table 1). As expected, the inhibitory activities against both wild-type and mutant EGFRs were weak due to the lack of Michael addition receptors

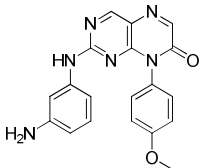
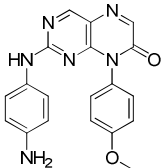
(Table 1). An acrylamide group was then added as a Michael addition receptor at the 4'- and 3'- positions of the N8-substituted phenyl ring to target Cys797 in EGFR on the basis of observing the overlay poses of NSC86929 and WZ4002. These efforts resulted in compounds **3a** and **3b**, which exhibited significantly increased inhibitory activities against wide-type, L858R mutant, and T790M/L858R mutant EGFR over those without the acrylamide group. Further saturation of the double bonds in the acrylamide group to form propanamides completely abolished the inhibitory activities against all the EGFR genotypes (**3a**, **3b** vs. **3c**, **3d**). However, the addition of acrylamide groups at the 4- and 3- positions of the NH-substituted ring also led to the suppression of the effectiveness of the inhibitors (**2e** and **2f**). All of these facts confirmed our initial hypothesis that introducing Michael addition receptors onto the novel pteridin-7(8*H*)-one scaffold can increase the EGFR binding affinity by mimicking the covalent binding mode of WZ4002 in the WT EGFR and the T790M mutant.

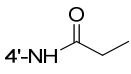
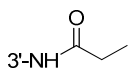
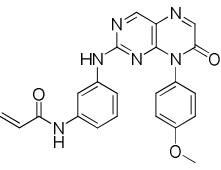
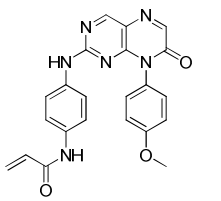
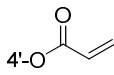
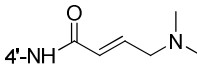
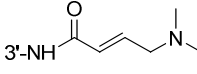
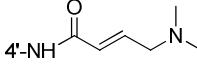
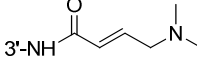
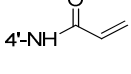
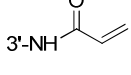
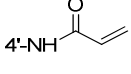
Scheme 1. Synthesis of pteridin-7(8*H*)-one derivatives^a



^aReagent and conditions: (a) ArNH₂, DIPEA, 1,4-dioxane, r.t., 65%-82%; (b) ArNH₂, DIPEA, 1,4-dioxane, r.t., 75%-85%; (c) Pd/C, H₂, EtOH, 83%-95%; (d) R₂COCOOEt, HOAc, EtOH,

Table 1. In Vitro Enzymatic Inhibitory Activities of Pteridin-7(8*H*)-one compounds^a

| Compounds | R1 | R2 | R3 | R4 | Enzyme Inhibitory Activity (IC50, nM) | | |
|-----------|-----|----|---|----|---------------------------------------|-------------|-------------|
| | | | | | WT | L858R | T790M/L858R |
| 2a | OMe | H | 4'-NH2 | H | NA ^b | NA | NA |
| 2b | OMe | H | 3'-NH2 | H | NA | 55920±24593 | 21280±664 |
| 2c | | |  | | 18280±4384 | 8039±1144 | 3836±395 |
| 2d | | |  | | 25825±2976 | 8452±1401 | 6754±768 |
| 3a | OMe | H | 4'-NH-C(=O)-CH=CH ₂ | H | 5129±2697 | 23747±3555 | 4802±3424 |
| 3b | OMe | H | 3'-NH-C(=O)-CH=CH ₂ | H | 13.8±4.8 | 14.8±4.2 | 5.6±2.5 |

| | | | | | | | |
|----|-----|---|---|---|-------------|-------------|-------------|
| 3c | OMe | H |  | H | NA | NA | NA |
| 3d | OMe | H |  | H | NA | NA | NA |
| 2e | | |  | | NA | NA | NA |
| 2f | | |  | | 33885±6993 | 70620±10012 | 70240±4666 |
| 3e | OMe | H |  | H | 60.4±7.6 | 122.6±3.5 | 59.1±13.6 |
| 3f | OMe | H |  | H | 59.1±1.6 | 76.5±21.4 | 31.3±7.4 |
| 3g | OMe | H |  | H | 26283±6520 | 32847±11188 | 56157±18543 |
| 3h | H | H |  | H | NA | NA | NA |
| 3i | H | H |  | H | 115.0±27.0 | 110.0±9.6 | 39.7±7.6 |
| 3j | H | H |  | H | NA | NA | NA |
| 3k | H | H |  | H | 12.80±2.21 | 11.10±1.97 | 4.94±0.48 |
| 3l | Cl | H |  | H | 373.5±186.3 | 496.0±163.0 | 144.1±27.7 |

1
2
3
4
5
6
7
8
9
10
11
12
13
14
15
16
17
18
19
20
21
22
23
24
25
26
27
28
29
30
31
32
33
34
35
36
37
38
39
40
41
42
43
44
45
46
47
48
49
50
51
52
53
54
55
56
57
58
59
60

| | | | | | | | |
|----|-----|----|--|-----|-------------|-------------|------------|
| 3m | Cl | H | | H | 47.10±5.74 | 49.10±2.62 | 17.60±2.81 |
| 3n | | H | | H | 5585±2983 | 8671±181 | 3456±628 |
| 3o | | H | | H | 6.95±0.89 | 7.26±1.24 | 2.86±0.29 |
| 3p | | H | | H | 1100±167 | 1510±207 | 691±76.8 |
| 3q | | H | | H | 1.21±0.27 | 1.32±0.10 | 0.677±0.15 |
| 3r | | H | | H | 15.7±3.6 | 14.8±3.4 | 5.12±0.55 |
| 3s | | H | | H | 15.3±6.9 | 13.0±0.36 | 4.96±0.4 |
| 3t | | H | | H | 14.5±7.9 | 14.1±2.0 | 4.72±0.85 |
| 3u | | H | | H | 12.5±2.9 | 14.0±0.7 | 4.53±0.5 |
| 3v | | H | | H | 12.1±0.7 | 11.8±1.9 | 3.97±0.86 |
| 3w | | H | | OMe | 395.0±66.8 | 496.0±144.0 | 272.0±47.0 |
| 3x | | H | | OMe | 3.82±0.23 | 2.56±0.23 | 1.07±0.13 |
| 3y | OMe | Me | | H | 16338±10170 | 7167±2963 | 35020±4140 |
| 3z | OMe | Me | | H | 5.29±1.7 | 5.73±0.39 | 13.0±0.26 |

WZ4002

2.16±0.33 3.82±0.23 0.66±0.15

^aEnzyme inhibitory activity assays were performed using the FRET-based Z'-Lyte assay, the detailed method was provided in the experimental section. All experiments were repeated at least three times.

^bNA: Not Active.

Structural Modification and SAR Interpretation. Because the addition of acrylamide moieties at different positions in compounds **3a** and **3b** resulted in remarkable differences in enzymatic inhibitory activities (compound **3b** was 300- to 1600-fold more potent against different types of EGFR than **3a**), we first investigated the impact of different Michael addition receptor groups. Replacing the acrylamide group with an acrylate group as Michael addition receptor (**3e**) was also able to inhibit different types of EGFR with even lower binding affinity. The addition of a dialkylaminomethyl group to the acrylamide fragment in clinical candidates such as EKB-569, BIBW2992, and HKI-272 has been reported to greatly increase their potency, which the dialkylamino group can serve as an intramolecular catalyst for the Michael addition reaction.^{11, 44} Inspired by this knowledge, we synthesized four compounds (**3f**, **3g**, **3h**, and **3i**) that possess a dialkylamino group attached to the acrylamide fragment. However, only **3f** displayed enhanced potency compared with the corresponding compounds (**3a**, **3b**, **3j**, and **3k**) that lacked the dialkylamino addition to the acrylamide moiety. On the other hand, the 3'-position of the N8-substituted phenyl ring is more favored than the 4'-position for acrylamide moiety modification by forming a covalent bond with Cys797 (**3b** vs. **3a**).

Next, we examined the impacts of variations in R¹ and R⁴ on the C2-position of the NH-substituted phenyl ring. The R¹ methoxy group in **3a** and **3b** were removed (**3j** and **3k**), or

replaced with halogen atoms (**3l** and **3m**), *N*-morpholino (**3n** and **3o**), or 1-(4-methylpiperazinyl) (**3p** and **3q**) groups, to evaluate the impact of the R¹ group. The results indicated that **3q** with a 1-(4-methylpiperazinyl) substituent exhibits the highest EGFR inhibitory potency, with IC₅₀ values against EGFR-WT, EGFR-L858R, and EGFR-T790M/L858R of 1.21, 1.32, and 0.677 nM, respectively. Further variants at the same position—1-piperidinyl (**3r**), 1-pyrrolidinyl (**3s**), diethylamino (**3t**), acetylamino (**3u**), and carbamoyl (**3v**)—did not improve the inhibitory activities. It has been reported that 4-methoxy is favored over 4-H on WZ4002 to enhance the selectivity over JAK3 and the TEC-family kinase, and replacing 4-methoxy with bulky but more lipophilic trifluoromethyl group decreases the activity by 6 folds.^{15, 45-46} The superposition of WZ4002 and NSC86929 in Figure 2B indicates that the aniline rings overlaid quite well and the 4-methoxy group can be tolerated in both compounds, which is believed to contribute to the hydrophobic interaction with hinge residues like L792. On the other hand, in our previous report that 2-oxo-3,4-dihydropyrimido[4,5-*d*]pyrimidinyl derivatives as the EGFR mutant inhibitors, replacing methoxy at the same corresponding position with larger ethoxy and isopropoxy groups both decrease the activities, while replacing with fluorol abolishes the activity completely.⁴⁵ Later SAR analysis by replacing 2-oxo-3,4-dihydropyrimido[4,5-*d*]pyrimidinyl scaffold with pyrimido[4,5-*d*]pyrimidin-4(1*H*)-one and 5,8-dioxo-pyrimido[4,5-*e*][1,4]diazepine indicates that methoxy is the most optimal group in terms of both activity and physiochemical properties at the corresponding position of R⁴ in the pteridin-7(8*H*)-one derivatives reported here.⁴⁷⁻⁴⁸ Herein the combination of an R⁴ methoxy group and a 1-(4-methylpiperazinyl) group leads to compound **3x**, which demonstrated improved solubility while maintaining a strong inhibition against EGFR-WT, EGFR-L858R, and EGFR-T790M/L858R with IC₅₀ values of 3.82, 2.56, and 1.07 nM, respectively (Figures S1-S3). We also attempted to introduce the R² methyl group (**3y**, **3z**) at the

C6-position. Compound **3y** lost its inhibitory potency for all EGFR types. The potency of **3z** against EGFR-WT and EGFR-L858R increased slightly over that of **3b**, while its binding affinity against EGFR-T790M decreased approximately 2-fold ($IC_{50} = 13.0$ nM).

Binding mode analysis. To investigate whether the added Michael acceptor can form the putative covalent bond with Cys797, which was intended to increase the binding affinities of the pteridin-7(8*H*)-one compounds, molecular docking was adopted to predict the binding modes of the representative potent compound **3q**. The covalent bond expected to form between the thiol of Cys797 and the acrylamide group was added as a spatial constraint in the docking simulation. The highest scoring (GoldScore is 44.09, whereas GoldScore of redocked WZ4002 is 50.85) binding pose for **3q** is shown in Figure 3. The compound binds tightly in the ATP-binding cleft of the EGFR T790M mutant, forming the expected covalent bond with the thiol of Cys797. The predicted binding pose corresponds well to the crystal structure of WZ4002 in the scaffold superposition between pteridin-7(8*H*)-one and pyridine (Figure 3A), which further coincides with the aligned poses generated with SHAFTS. The pteridin-7(8*H*)-one core forms a bidentate hydrogen bonded interaction with the ‘hinge’ residues Met793 and Pro794 (Figure 3B), and the double-ring system contacts the mutant gatekeeper residue, Met790. Although this hydrophobic contact is not as tight as that of the chlorine substituent on the pyrimidine ring in WZ4002, it is still likely to contribute to the potency of these compounds toward the T790M mutant, as demonstrated by the high inhibitory activities for the EGFR T790M mutant. Due to the constraint imposed by the double-ring conformation, the aniline ring was oriented to form hydrophobic interactions with Leu792 and Pro794 in the hinge region. This orientation, in turn, allows the addition of OMe at the R⁴ position to create a hydrophobic contact with the backbone of the hinge region as in compound **3x**. Moreover, as with WZ4002, the “linker” phenyl ring lies

roughly perpendicular to the pteridin-7(8*H*)-one core; this orientation juxtaposes the acrylamide with the thiol of Cys797 to permit the formation of a covalent bond and causes the acrylamide moiety to prefer the 3'-position over the 4'-position.

The addition of a dialkylaminomethyl group to the acrylamide fragment in clinical candidates has been reported to greatly increase their potency; however none of the dialkylamino derivatives reported herein displayed equivalent binding affinities to that of **3x**. Moreover it is even confusing that 3'-acrylamide is preferred in general except in the cases of **3g** and **3f**, where the 4'-substitution is more preferred, indicating alternative binding poses exist for these dialkylamino derivatives. Further docking analysis was performed for the dialkylamino derivatives **3f-3i** (Figure S4). On the basis of docking analysis, in most of the cases like **3q**, 3'-acrylamide is more favored because it can be attacked by the thiol of Cys797 due to the proper orientation as shown in Figure 3B and therefore binds as a potent covalent inhibitor. The 4'-acrylamide, on the other hand, is too far to be reached by Cys797 and thus all the compounds hosting 4'-acrylamide are actually bound as non-covalent inhibitors, of which the activities were expected to be worse than the covalent ones. However, in the cases of **3g** and **3i**, despite that the Michael receptors are at 3' position, the dialkylamino-attached acrylamide is more bulky than acrylamide alone, and cause severe steric clashes with Leu799 and Arg841 if forced to form the covalent bonds as observed in other 3'-acrylamide compounds. Therefore they are unlikely to bind as covalent inhibitors. Molecular docking suggests the 3'-dialkylamino-attached acrylamide of **3i** may extend to the subpocket near the salt bridge formed by Lys745 and Asp855 as shown in Figure S4A. While the 4-OMe of **3g** tends to attract the 3'-dialkylamino-attached acrylamide by forming intra-molecular hydrophobic patch and therefore forces the molecule into a U-shaped conformation, which makes it impossible to maintain the key hydrogen bonds with the hinge

residues (as shown in Figure S4B) and abolish the binding remarkably. As to **3h** and **3f**, the docking analysis suggests they are likely to form the same U-shaped conformations as shown in Figures S4C and S4D, in which the 4'-dialkylamino-attached acrylamide can form a charged interaction with Asp800. The binding energies are very similar. However, the energies of these two conformations in the unbound state are significantly different: the binding strain energy of **3f** is nearly 30 kJ/mol lower than that of **3h**. Similar to that of **3g**, the 4-OMe in **3f** tends to attract 4'-dialkylamino-attached acrylamide by intra-molecular hydrophobic patch and stabilizes the U-shaped conformation even in the unbound state. Therefore for **3h**, the binding energy is massively offset by the strain energy of the ligand, leading to a much lower activity than that of **3f**.

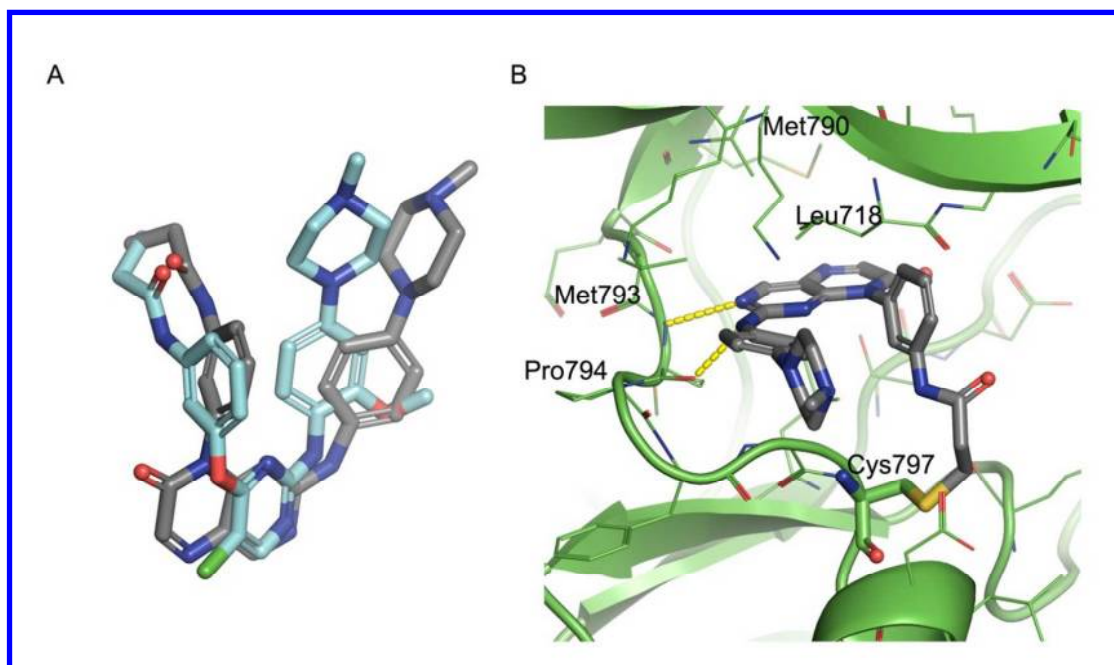


Figure 3. (A) Schematic diagram of the predicted binding pose of **3q** (dark grey) and the crystal structure of WZ4002 (cyan) binding in an EGFR T790M mutant. (B) Docking pose of **3q** in a complex with the EGFR T790M mutant (PDB ID 3IKA). The EGFR kinase is shown in a cartoon representation (green) with the bound inhibitor in a stick representation (dark grey). The

sidechain and mainchain atoms are shown for selected residues that contact the compound. The expected hydrogen bonds with the backbone amide and the carbonyl atoms of Met793 and Pro794 are indicated by the dashed yellow lines. Note the covalent bond with Cys797, which is also shown in the stick representation.

Selectivities and Cellular Activities of Compounds 3x. To further assess the specificity of one of the most potent compounds **3x**, we profiled the compound' inhibitory activities against a panel of 387 wildtype kinases covering a majority of the kinase families across the whole kinome using DiscoverX's KINOMEscan platform (Figure 4, Table S1).⁴⁹ Given that the special mechanism of the covalent kinase inhibitors targeting cysteine at specific positions, the selectivity of such type of inhibitors can be high as widely reported. The selectivity profile of compound **3x** is excellently given that only BTK and HER4 (ERBB4) show similar strong binding interaction to the EGFR mutants (percent control value < 1%). Other off-targets showing weaker binding includes wildtype EGFR, HER2 (ERBB2), and JAK3 (percent control value < 10%). It is not surprising that all the potential off-targets are tyrosine receptor kinases harboring a cysteine structurally corresponding to Cys797 in EGFR and its mutants. Moreover, compound **3x** did show some selectivity for JAK3 (percent control value 7%) over EGFR T790M, L858R, and T790M/L858R mutants (percent control values 0.35%, 0.3%, and 0.1%, respectively) with the combination of an R⁴ methoxy group and a 1-(4-methylpiperazinyl) group, corresponding well to the aforementioned design strategy. The high selectivity of compounds indicates less off-target effects and potential safety index for further development.

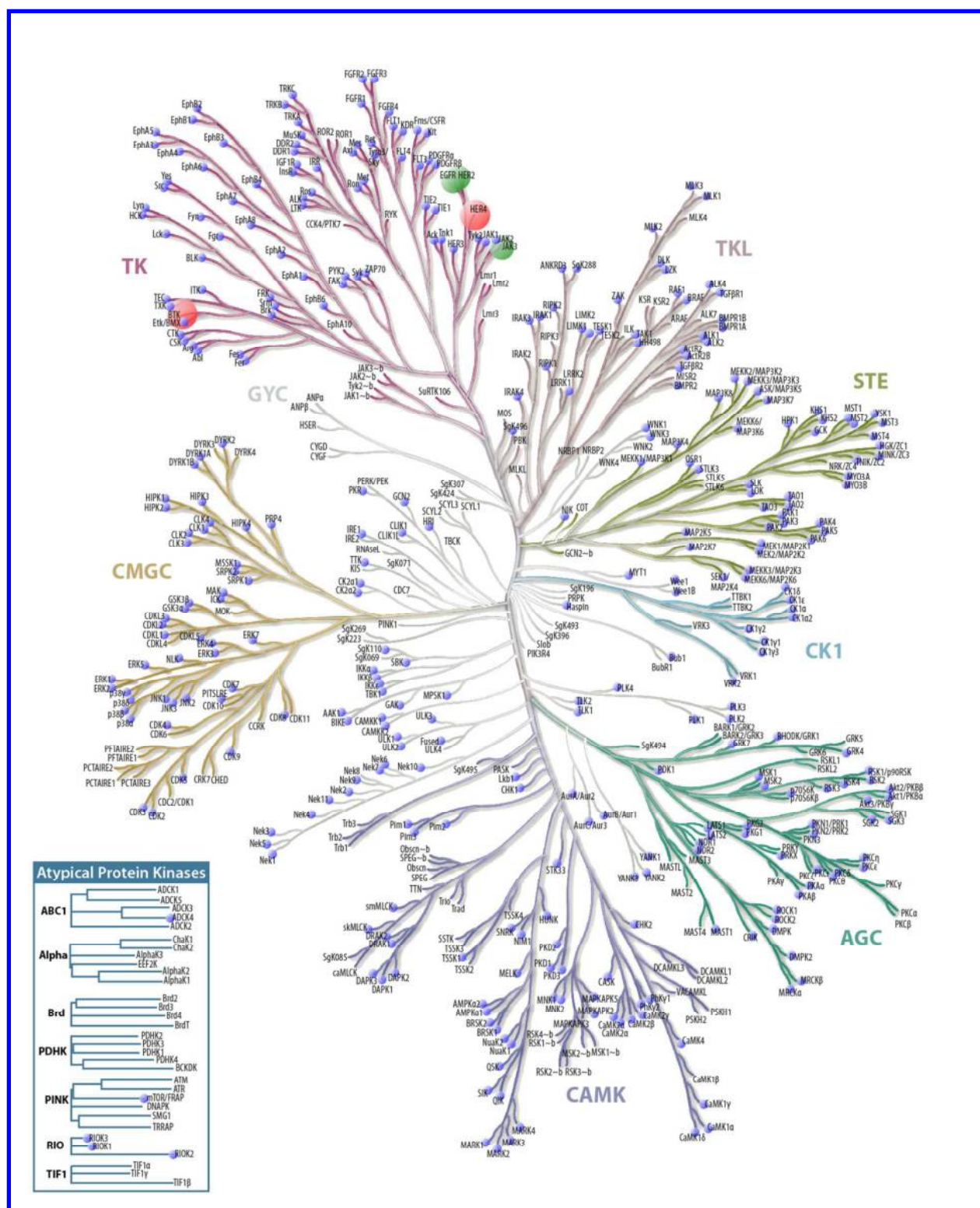


Figure 4. Selectivity profiles for compounds **3x** versus a panel of 387 wildtype kinase targets.

The color and size of the circle designates the KINOMEScan (www.discoverx.com) results of **3x**

at 1 μ M concentration, where the results for primary screen binding interactions are reported as percent control values ('%Control', see Supporting Information), where lower numbers indicate stronger bindings: < 1% (red), 1–10% (green), and > 10% (blue), respectively. The kinome tree illustration was adapted with permission from Cell Signaling Technology, Inc (www.cellsignal.com).

To further assess the tumor suppression effects of these novel EGFR inhibitors, their cellular antiproliferative activities were investigated (Table 2), and the results were highly consistent with their enzyme inhibitory activities. Compounds **2a**, **2b**, **2c**, **2d**, **3c**, and **3d**, which did not inhibit any enzyme activity, exhibited weak antiproliferative effects on both the gefitinib-sensitive HCC827 cells (harboring EGFR-delE746_A750) and gefitinib-resistant H1975 cells (expressing EGFR-T790M/L858R), due to the low binding affinities for both wildtype and T790M/L858R mutant EGFR as previously described. The most enzymatically potent compounds **3b**, **3q**, and **3x** also exhibited potent growth-inhibitory activities in the HCC827 cells with IC₅₀ values of 9 nM, 4 nM and 8 nM, respectively, and were thus equally potent to that of gefitinib. More importantly, compounds **3q** and **3x** displayed high inhibitory activities against the growth of gefitinib-resistant H1975 cells, similar to the effects of WZ4002. It is notable that compounds **3x** and **3z** showed similar enzyme inhibitory activities in EGFR-WT (3.82 vs. 5.29 nM) and EGFR-L858R mutant (2.56 vs. 5.73 nM), but the cellular activity of **3x** in H1975 cell line is ~35 fold higher than that of **3z**. Because **3x** was ~12 fold more active than **3z** in EGFR-T790M/L858R double mutant in terms of enzymatic inhibitory activity (1.07 vs. 13.0 nM) and H1975 cell line primarily harbors EGFR-T790M/L858R double mutants, the cellular activity gap between **3x** and **3z** in H1975 cells can be attributed to this selectivity to different EGFR mutant

types correspondingly. The other compounds exhibited moderate potency in suppressing the growth of HCC827 cells or H1975 cells. These results correspond very well with our design hypothesis and the predicted binding modes.

Table 2. Cellular antiproliferative activities of Pteridin-7(8*H*)-One Compounds^a

| Compounds | Cellular Antiproliferative Activity (IC ₅₀ , nM) | |
|-----------|---|-----------|
| | HCC827 | H1975 |
| 2a | NA ^b | NA |
| 2b | NA | NA |
| 2c | NA | NA |
| 2d | NA | NA |
| 2e | 1217±107 | 2364±265 |
| 2f | 1457±434 | 1330±87 |
| 3a | 1688±248 | 2198±420 |
| 3b | 9.49±1.79 | 63.8±13.4 |
| 3c | NA | NA |
| 3d | NA | NA |
| 3e | 8589±2265 | 5901±915 |
| 3f | 8378±606 | NA |
| 3g | 917±229 | 559±107 |
| 3h | 5007±476 | NA |
| 3i | 1294±461 | 4963±1732 |

1
2
3
4
5
6
7
8
9
10
11
12
13
14
15
16
17
18
19
20
21
22
23
24
25
26
27
28
29
30
31
32
33
34
35
36
37
38
39
40
41
42
43
44
45
46
47
48
49
50
51
52
53
54
55
56
57
58
59
60

| | | |
|------------------|------------------|------------------|
| 3j | NA | NA |
| 3k | 53.1±34.1 | 562±195 |
| 3l | NA | NA |
| 3m | 175±14 | 2238±660 |
| 3n | 7163±703 | NA |
| 3o | 15.2±1.9 | 255±117 |
| 3p | 2370±585 | 6145±2015 |
| 3q | 4.02±1.52 | 62.2±24.2 |
| 3r | 25.3±5.0 | 298±108 |
| 3s | 70.8±3.8 | 579±120 |
| 3t | 44.5±15.5 | 4087±1152 |
| 3u | 388±123 | 4080±1656 |
| 3v | 511±101 | 8481±2792 |
| 3w | 503±124 | 2742±143 |
| 3x | 8.60±5.55 | 59.0±25.9 |
| 3y | 2758±451 | NA |
| 3z | 25.9±12.8 | 3518±1451 |
| WZ4002 | 12.4±3.4 | 48.7±8.9 |
| Gefitinib | 5.81±1.89 | 13613±434 |

^aThe Cellular antiproliferative activities were assessed using an MTS assay, the detailed method was provided in the experimental section. All experiments were repeated at least four times.

^bNA: Not Active (IC50 > 10 μM).

***In vivo* antitumor effect of compound 3x.** Antitumor efficacy of Compound **3x** was evaluated on a NSCLC xenograft mouse model of H1975 (EGFR-T790M/L858R) *in vivo* (Figure 5). Mice were dosed with **3x** at 20 or 40 mg/kg, IP, qd (intraperitoneal injection, once every day) for 14 days. Both doses of **3x** were well tolerated, with no mortality or significant body weight loss (<5% relative to the vehicle matched controls) observed during the treatment (Figure S5). Compound **3x** displayed significant antitumor efficacy *in vivo* ($p < 0.05$) and induced tumor stasis even at 20 mg/kg/day, which indicates that it might serve as a promising lead compound for further development as an EGFR inhibitor to overcome EGFR-T790M mutation-related clinical resistance to gefitinib or erotinib.

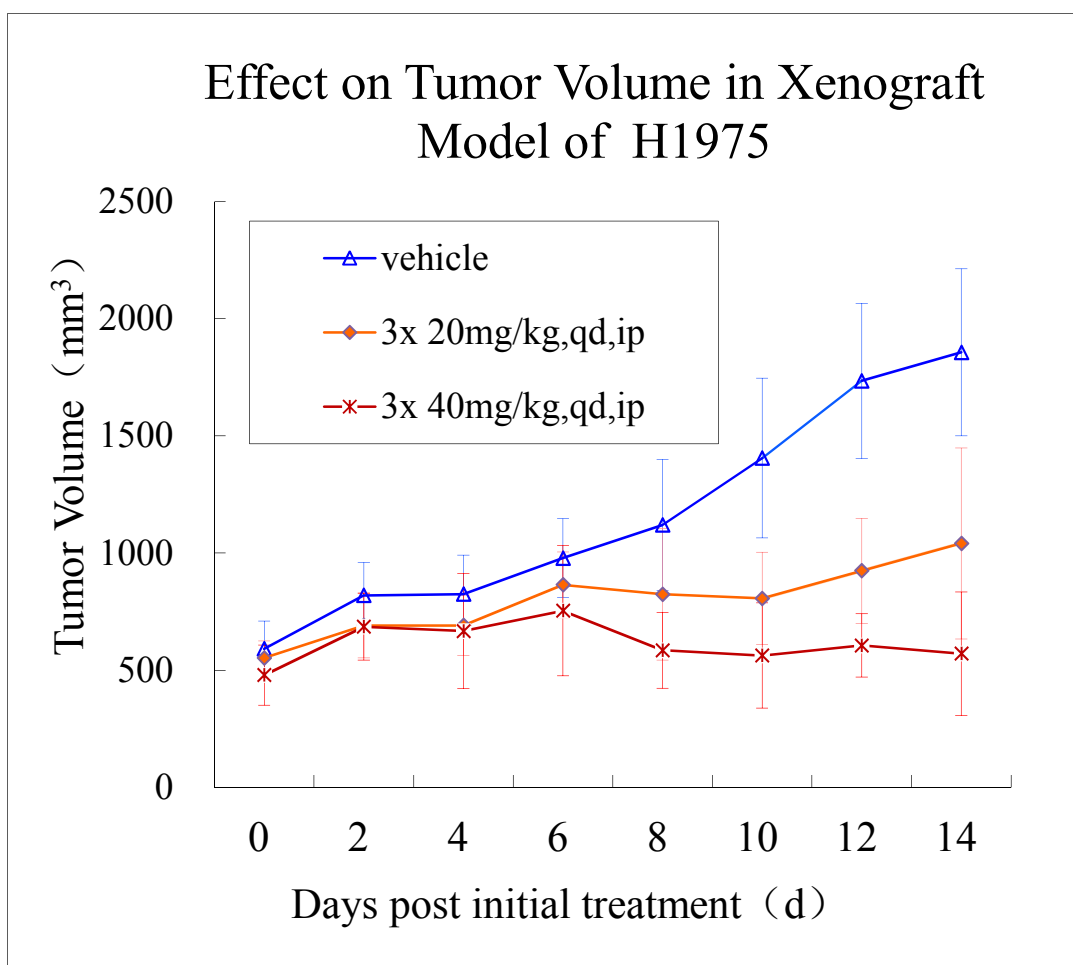


Figure 5. *In vivo* antitumor effect of compound **3x** in a human NSCLC (H1975) xenograft nude mouse model. Mice were monitored for signs of morbidity (behavior and body loss), and tumors were measured every other day. Statistical significance ($p < 0.05$) for antitumor efficacy, based upon tumor growth relative to the vehicle controls. None animal died during the treatment.

CONCLUSION

In this study, we highlighted the importance of molecular 3D similarity calculations in drug design by discovering a novel pteridin-7(8*H*)-one scaffold for irreversible EGFR inhibitors using a computational scaffold-hopping strategy. To discover irreversible inhibitors with novel scaffold based on previous research on the conversion of a pyrimidine scaffolds-based EGFR inhibitor to an irreversible EGFR T790M mutant inhibitor, an in-house molecular 3D similarity calculation program, SHAFTS, was used to search the NCI database for an alternative scaffold. This search led to the discovery of a novel pteridin-7(8*H*)-one EGFR inhibitor scaffold. As expected, further conversion of the new scaffold into an irreversible inhibitor was achieved by introducing Michael addition receptor groups. This addition led to highly potent EGFR T790M mutant inhibitors that exhibited competitive inhibitory enzymatic activities with sub-nanomolar IC_{50} values against both wild-type and T790M/L858R mutant EGFRs. The most active compounds, **3q** and **3x**, strongly inhibited the growth of gefitinib-resistant H1975 cells. Kinase selectivity profiling revealed that one of the most effective compounds **3x** is highly selective to EGFR and corresponding mutants, indicating a good safety index. Moreover, further *in vivo* antitumor efficacy study demonstrated that compound **3x** significantly inhibited the tumor growth and induced tumor stasis in an EGFR-T790M/L858R driven human NSCLC xenograft mouse model of H1975 by IP dosing at 20 mg/kg/day. In conjunction with the binding mode prediction data, these results suggest that the novel pteridin-7(8*H*)-one based inhibitors utilize

1
2
3 the same mode of action as the patent- protected pyridine inhibitors. Our investigations
4
5 demonstrate the pivotal roles of molecular shape and chemotype and matching in scaffold
6
7 hopping and demonstrate the use of molecular 3D calculations to provide a novel starting point
8
9 with which to generate competitive bioactivities.
10
11
12
13
14
15
16
17
18
19
20
21
22
23
24
25
26
27
28
29
30
31
32
33
34
35
36
37
38
39
40
41
42
43
44
45
46
47
48
49
50
51
52
53
54
55
56
57
58
59
60

EXPERIMENTAL SECTION

Computational Protocol. Using the reported bioactive conformation of WZ4002 (with Michael addition receptor deleted) in the EGFR T790M crystal structure (PDB code 3IKA) as the query, SHAFTS was utilized to search the NCI databases. SHAFTS employs a hybrid similarity metric of molecular shape and colored (labeled) chemical groups annotated as pharmacophore features for the 3D similarity calculation and ranking. This approach is designed to integrate the strength of both the pharmacophore matching and volumetric similarity approaches. The details of the algorithm and application are provided elsewhere and can be accessed at the ChemMapper Server.⁵⁰

Because SHAFTS uses a semi-rigid strategy to characterize molecular flexibility, Cyndi, a previously described multi-objective evolution algorithm based conformational analysis program,⁵¹ was used to generate multiple conformers (a maximum of 200 lowest-energy conformers) for each molecule in the databases. The top-ranked molecules with SHAFTS similarities > 1.0 (maximum 2.0) were reserved. Presumably the two benzene rings attached on the pyrimidine scaffold are preferred to be reserved for introducing Michael addition receptor. According to these selection criteria, the highest ranked compound, compound **2** with the pteridin-7(8*H*)-one core replacing the pyrimidine core, was identified as the most appropriate scaffold for further chemical modification. The entire calculation process was simply performed submitting a job to the ChemMapper server, and the structures and SHAFTS similarity scores for all the top ranked hits can be accessed at the same website using the job ID of 10485 (<http://lilab.ecust.edu.cn/chemmapper/result/getResult.html?jobId=10485>).

Covalently bound docking of compound **3q** was performed with GOLD (version 4.0; Cambridge Crystallographic Database: Cambridge, U.K., 2008). The structure of the EGFR

T790M mutant complexed with WZ4002 (PDB code: 3IKA) was used as the receptor. The receptor model was prepared using a standard protein setup protocol, which included removing all crystal water molecules and the bound WZ4002 ligand, adding hydrogen atoms, and correcting the ionization and tautomeric states of residues such as Asp, Glu, and His. The binding site was defined as the residues surrounding the WZ4002 molecule. The covalent bond was manually defined using the interactions between the sulfur atom on the Cys797 thiol and the terminal carbon atom on the acrylamide group of **3q** as constraints. To achieve this goal, the chemical structure of the ligand **3q** was slightly modified: the double bond in the acrylamide group was saturated and attached to the terminal sulfur atom as the “link atom”. During the GOLD docking simulation, the link atom in the ligand was forced to fit onto the sulfur atom of Cys797 in the protein to mimic covalent bonding.

The non-covalent docking of compounds **3f-3i** was performed with Glide (Schrödinger, Inc.) in standard precision (SP) mode. The receptor model was prepared with Protein Preparation Wizard and the four ligands were prepared with LigPrep module in Maestro. The grid-enclosing box was centered on the centroid of WZ4002 in the same EGFR crystal structure mentioned above and defined so as to enclose residues located within 14.0 Å around the ATP binding site, and a scaling factor of 1.0 was set to van der Waals (VDW) radii of those receptor atoms with the partial atomic charge less than 0.25. The top one ranked poses for each ligand were taken for interaction mode analysis.

Reagents and General Methods. All chemical reagents and solvents were purchased from commercial sources and used without further purification. Thin-layer chromatography (TLC) was performed on silica gel plates. Column chromatography was performed using 200-300 mesh silica gel (Hailang, Qingdao). The ¹H and ¹³C NMR spectra were recorded on a Bruker AV-400

spectrometer with chemical shifts expressed in parts per million (in DMSO-*d*₆ or CDCl₃, using Me₄Si as the internal standard). Melting points were determined using an X-6 micro-melting point apparatus. The mass spectra were measured at the Institute of Fine Chemistry of ECUST. The purities of all final compounds were analyzed via HPLC, with the purity all being higher than 95%. The analytical HPLC was performed on a Hewlett-Packard 1100 system chromatograph equipped with a photodiode array detector using a Zorbax RX-C18 5 μm, 250 mm × 4.6 mm column (reverse phase). The mobile phase was a gradient of 90-100% methanol (solvent 1) and 10mM NH₄OAc in water (pH 6.0) (solvent 2) at a flow rate of 1.0 mL/min (0-1.0 min, 90% solvent 1; 1.0-15.0 min, 90-100% solvent 1; 15.0-20.0 min, 100-90% solvent 1).

General Synthesis of the Pteridin-7(8*H*)-One Compounds. The pteridin-7(8*H*)-one analogues used in this study were synthesized as shown in Scheme 1. Condensation of commercially available 2,4-dichloro-5-nitro-pyrimidine (**4**) with a primary arylamine in 1,4-dioxane containing N,N-Diisopropylethylamine (DIPEA) provided intermediates with structure **5**. Compound **6** was prepared from intermediate **5** via nucleophilic substitution with another arylamine. The nitro group in compound **6** was reduced with Pd/C using hydrogenation in ethanol to obtain compound **7** with a nucleophilic amino group in good yields. The diaminopyrimidine compound **7** was cyclized with ethyl glyoxalate (or ethyl pyruvate) and acetic acid under refluxing with ethanol to form the pteridin-7(8*H*)-one core in compound **8**.⁵² Compound **8** was deprotected with trifluoroacetic acid in dichloromethane and further acylated by the corresponding acyl chloride to yield the pteridin-7(8*H*)-one derivatives. The detailed synthetic method and characterization are provided in the Supporting Information.

tert-butyl 4-(2-chloro-5-nitropyrimidin-4-ylamino)phenylcarbamate (5a): To solution of 2,4-dichloro-5-nitro-pyrimidine (95 mg, 0.49 mmol) in 1,4-dioxane (3 mL) was added a solution of tert-butyl 4-aminophenylcarbamate (100 mg, 0.48 mmol) in 1,4-dioxane (2 mL) and DIPEA (69 mg, 0.53 mmol). The reaction mixture was stirred at room temperature for 2 h. The solvent was removed in vacuo and crude product was purified by flash silica gel chromatography (petroleum ether/ethylacetate = 10/1, v/v) to obtain the title product as a yellow solid (144 mg, 82%). ¹H NMR (400 MHz, DMSO-*d*₆): δ 10.38 (s, 1H), 9.46 (s, 1H), 9.12 (s, 1H), 7.49 (d, *J* = 8.6 Hz, 2H), 7.39 (d, *J* = 8.6 Hz, 2H), 1.49 (s, 9H).

tert-butyl 4-(2-(4-methoxyphenylamino)-5-nitropyrimidin-4-ylamino)phenylcarbamate(6a): To a solution of compound **5a** (50 mg, 0.14 mmol) in 1,4-dioxane was added 4-methoxyaniline (17 mg, 0.14 mmol) and DIPEA (18 mg, 0.18 mmol). The reaction mixture was stirred at room temperature for 4 h. The solvent was removed in vacuo and crude product was purified by flash silica gel chromatography (petroleum ether/ethylacetate = 4/1, v/v) to obtain the title product as a yellow solid (51 mg, 82%). ¹H NMR (400 MHz, DMSO-*d*₆): δ 10.30 (s, 1H), 10.26 (s, 1H), 9.45 (s, 1H), 9.04 (s, 1H), 7.49 (d, *J* = 8.8 Hz, 2H), 7.45 (d, *J* = 8.8 Hz, 2H), 7.40 (d, *J* = 8.6 Hz, 2H), 6.75 (d, *J* = 8.6 Hz, 2H), 3.73 (s, 3H), 1.50 (s, 9H).

tert-butyl 4-(5-amino-2-(4-methoxyphenylamino)pyrimidin-4-ylamino)phenylcarbamate (7a): A solution of compound **6a** (45 mg, 0.10 mmol) in ethanol (20 mL) was treated with 10% palladium on charcoal (10 wt. %) and hydrogenated at 30 psi for 12 h. The catalyst was filtered through celite and filtrate was concentrated under reduced pressure. The resulting crude product was purified by flash silica gel chromatography (dichloromethane/methanol = 5/1, v/v) to obtain the title product as a white solid (30 mg, 83%). ¹H NMR (400 MHz, DMSO-*d*₆): δ 9.23 (s, 1H),

8.42 (s, 1H), 8.10 (s, 1H), 7.62 (d, $J = 9.2$ Hz, 2H), 7.56 (s, 1H), 7.53 (d, $J = 9.2$ Hz, 2H), 7.40 (d, $J = 8.8$ Hz, 2H), 6.77 (d, $J = 8.8$ Hz, 2H), 3.70 (s, 3H), 1.48 (s, 9H).

***tert*-butyl 4-(2-(4-methoxyphenylamino)-7-oxopteridin-8(7*H*)-yl)phenylcarbamate (8a):**

To a solution of compound **7a** (30 mg, 0.07 mmol) in acetic acid (0.29 mL) and ethanol (5 mL) was added a solution of ethyl glyoxylate in toluene (ca. 50%) (16 mg, 0.08 mmol). The reaction mixture was stirred at reflux for 12 h and concentrated. The residue was triturated with ammonia water and filtered. The filter cake was washed with water and dried to obtain the title compound as a yellow solid (18 mg, 76%). ^1H NMR (400 MHz, DMSO- d_6): δ 10.08 (s, 1H), 9.64 (s, 1H), 8.84 (s, 1H), 8.03 (s, 1H), 7.65 (d, $J = 8.4$ Hz, 2H), 7.30-7.28 (m, 4H), 6.61 (br, 2H), 3.67 (s, 3H), 1.52 (s, 9H).

8-(4-aminophenyl)-2-(4-methoxyphenylamino)pteridin-7(8*H*)-one (2a): To a solution of compound **8a** (18 mg, 0.04 mmol) in dichloromethane (2 mL) was added trifluoroacetic acid (0.5 mL) at 0 °C. The reaction mixture was stirred for 2 h at room temperature. The reaction mixture was partitioned between dichloromethane (20 mL) and saturated NaHCO₃ (10 mL), the water layer was extracted with dichloromethane (10 mL \times 2). The combined organic layer was washed with water and brine, dried over Na₂SO₄, the solid was filtered off, and the filtrate was concentrated under reduced pressure. The resulting crude product was purified by flash silica gel chromatography (dichloromethane/methanol = 30/1, v/v) to obtain the title product as a yellow solid (13 mg, 92%), mp >300 °C. ^1H NMR (400 MHz, DMSO- d_6): δ 10.04 (br, 1H), 8.81 (s, 1H), 8.00 (s, 1H), 7.40 (d, $J = 7.6$ Hz, 2H), 6.98 (d, $J = 8.4$ Hz, 2H), 6.73 (d, $J = 8.4$ Hz, 2H), 6.67 (br, 2H), 5.44 (s, 2H), 3.70 (s, 3H). ^{13}C NMR (100 MHz, DMSO- d_6): δ 159.19, 158.53, 157.17, 154.95, 151.76, 149.66, 146.68, 133.17, 129.22, 122.66, 121.04, 120.70, 114.37, 113.87, 55.55.

HPLC purity: 97.6%, Retention time = 12.59 min. HRMS (ESI): exact mass calcd for $C_{19}H_{17}N_6O_2$ $[M+H]^+$, 361.1413, found 361.1414.

***N*-(4-(2-(4-methoxyphenylamino)-7-oxopteridin-8(7*H*)-yl)phenyl)acrylamide (3a):** To a solution of compound **2a** (100 mg, 0.28 mmol) in triethylamine (28 mg, 0.28 mmol) and dichloromethane (50 mL) was added a solution of acryloyl chloride (29 mg, 0.31 mmol) in dichloromethane (5 mL) at 0 °C. The reaction mixture was stirred for 12 h at room temperature. The solvent was removed in vacuo and crude product was purified by flash silica gel chromatography (dichloromethane/ethylacetate = 5/1, v/v) to obtain the title product as a yellow solid (34 mg, 30%), mp 292.5-293.2 °C. 1H NMR (400 MHz, DMSO- d_6): δ 10.42 (s, 1H), 10.07 (br, 1H), 8.84 (s, 1H), 8.04 (s, 1H), 7.87 (d, J = 8.8 Hz, 2H), 7.38 (d, J = 8.8 Hz, 2H), 7.30 (br, 2H), 6.59 (br, 2H), 6.52 (dd, J = 17.0, 10.0 Hz, 1H), 6.33 (dd, J = 17.0, 1.8 Hz, 1H), 5.82 (dd, J = 10.0, 1.8 Hz, 1H), 3.62 (s, 3H). ^{13}C NMR (100 MHz, DMSO- d_6): δ 163.90, 159.28, 158.51, 156.68, 155.02, 151.44, 146.65, 139.72, 133.00, 130.18, 129.50, 127.72, 121.02, 120.61, 113.77, 55.40. HPLC purity: 95.5%, Retention time = 13.07 min. HRMS (ESI): exact mass calcd for $C_{22}H_{19}N_6O_3$ $[M+H]^+$, 415.1519, found 415.1515.

The following compounds (**2b-d**) and compounds (**2e**, **2f**, **3b-z**) were prepared by a method similar to that for compound **2a** and compound **3a**, respectively.

8-(3-aminophenyl)-2-(4-methoxyphenylamino)pteridin-7(8*H*)-one (2b): Yellow solid (yield 86%), mp 270.5-270.9 °C. 1H NMR (400 MHz, DMSO- d_6): δ 10.06 (br, 1H), 8.83 (s, 1H), 8.01 (s, 1H), 7.41 (d, J = 8.0 Hz, 2H), 7.22 (t, J = 8.0 Hz, 1H), 6.75 (d, J = 7.6 Hz, 1H), 6.67 (br, 2H), 6.53 (s, 1H), 6.48 (d, J = 7.6 Hz, 1H), 5.35 (s, 2H), 3.69 (s, 3H). HPLC purity: 94.4%, Retention time = 12.90 min. HRMS (ESI): exact mass calcd for $C_{19}H_{17}N_6O_2$ $[M+H]^+$, 361.1413, found 361.1413.

2-(3-aminophenylamino)-8-(4-methoxyphenyl)pteridin-7(8H)-one (2c): Yellow solid (yield 85%), mp 244.5-245.4 °C. ¹H NMR (400 MHz, DMSO-*d*₆): δ 9.91 (s, 1H), 8.85 (s, 1H), 8.04 (s, 1H), 7.35 (d, *J* = 8.8 Hz, 2H), 7.16 (d, *J* = 8.8 Hz, 2H), 6.68-6.65 (m, 3H), 6.16 (d, *J* = 7.2 Hz, 1H), 4.63 (s, 2H), 3.86 (s, 3H). HPLC purity: 98.9%, Retention time = 12.57 min. HRMS (ESI): exact mass calcd for C₁₉H₁₇N₆O₂ [M+H]⁺, 361.1413, found 361.1411.

2-(4-aminophenylamino)-8-(4-methoxyphenyl)pteridin-7(8H)-one (2d): Yellow solid (yield 88%), mp 281.5-282.3 °C. ¹H NMR (400 MHz, DMSO-*d*₆): δ 9.87 (s, 1H), 8.77 (s, 1H), 7.97 (s, 1H), 7.32 (d, *J* = 8.8 Hz, 2H), 7.13 (d, *J* = 8.8 Hz, 2H), 7.08 (br, 2H), 6.24 (br, 2H), 4.84 (s, 2H), 3.88 (s, 3H). HPLC purity: 95.2%, Retention time = 11.91 min. HRMS (ESI): exact mass calcd for C₁₉H₁₇N₆O₂ [M+H]⁺, 361.1413, found 361.1417.

N-(3-(8-(4-methoxyphenyl)-7-oxo-7,8-dihydropteridin-2-ylamino)phenyl)acrylamide (2e): Yellow solid (yield 73%), mp 243.3-244.0 °C. ¹H NMR (400 MHz, DMSO-*d*₆): δ 10.17 (s, 1H), 10.01 (s, 1H), 8.89 (s, 1H), 8.07 (s, 1H), 7.63 (br, 1H), 7.33 (d, *J* = 8.8 Hz, 2H), 7.27 (d, *J* = 8.0 Hz, 1H), 7.23 (d, *J* = 8.0 Hz, 1H), 7.11 (d, *J* = 8.8 Hz, 2H), 6.89 (br, 1H), 6.46 (dd, *J* = 17.0, 10.2 Hz, 1H), 6.25 (dd, *J* = 17.0, 1.8 Hz, 1H), 5.74 (dd, *J* = 10.2, 1.8 Hz, 1H), 3.85 (s, 3H). HPLC purity: 99.0%, Retention time = 12.91 min. HRMS (ESI): exact mass calcd for C₂₂H₁₉N₆O₃ [M+H]⁺, 415.1519, found 415.1519.

N-(4-(8-(4-methoxyphenyl)-7-oxo-7,8-dihydropteridin-2-ylamino)phenyl)acrylamide (2f): Yellow solid (yield 77%), mp 275.3-276.4 °C. ¹H NMR (400 MHz, DMSO-*d*₆): δ 10.19 (br, 1H), 10.03 (s, 1H), 8.87 (s, 1H), 8.05 (s, 1H), 7.36-7.34 (m, 6H), 7.16 (d, *J* = 8.4 Hz, 2H), 6.41 (dd, *J* = 17.0, 10.2 Hz, 1H), 6.23 (dd, *J* = 17.0, 1.6 Hz, 1H), 5.72 (dd, *J* = 10.2, 1.6 Hz, 1H), 3.92 (s, 1H). HPLC purity: 96.9%, Retention time = 12.75 min. HRMS (ESI): exact mass calcd for C₂₂H₁₉N₆O₃ [M+H]⁺, 415.1519, found 415.1524.

***N*-(3-(2-(4-methoxyphenylamino)-7-oxopteridin-8(7*H*)-yl)phenyl)acrylamide (3b):** Yellow solid (yield 74%), mp 260.9-261.5 °C. ¹H NMR (400 MHz, DMSO-*d*₆): δ 10.42 (s, 1H), 10.10 (br, 1H), 8.85 (s, 1H), 8.05 (s, 1H), 7.84 (d, *J* = 8.0 Hz, 1H), 7.78 (s, 1H), 7.56 (t, *J* = 8.0 Hz, 1H), 7.31 (br, 2H), 7.13 (d, *J* = 8.0 Hz, 1H), 6.58 (br, 2H), 6.45 (dd, *J* = 16.8, 10.4 Hz, 1H), 6.26 (dd, *J* = 16.8, 1.6 Hz, 1H), 5.77 (dd, *J* = 10.4, 1.6 Hz, 1H), 3.65 (s, 3H). HPLC purity: 97.0%, Retention time = 13.11 min. HRMS (ESI): exact mass calcd for C₂₂H₁₉N₆O₃ [M+H]⁺, 415.1519, found 415.1516.

***N*-(4-(2-(4-methoxyphenylamino)-7-oxopteridin-8(7*H*)-yl)phenyl)propionamide (3c):** Yellow solid (yield 78%), mp 258.5-259.1 °C. ¹H NMR (400 MHz, DMSO-*d*₆): δ 10.15 (s, 1H), 10.08 (br, 1H), 8.85 (s, 1H), 8.04 (s, 1H), 7.80 (d, *J* = 8.4 Hz, 2H), 7.35-7.33 (m, 4H), 6.61 (br, 2H), 3.67 (s, 3H), 2.41 (q, *J* = 7.6 Hz, 2H), 1.14 (t, *J* = 7.6 Hz, 3H). HPLC purity: 99.3%, Retention time = 13.05 min. HRMS (ESI): exact mass calcd for C₂₂H₂₁N₆O₃ [M+H]⁺, 417.1675, found 417.1674.

***N*-(3-(2-(4-methoxyphenylamino)-7-oxopteridin-8(7*H*)-yl)phenyl)propionamide (3d):** Yellow solid (yield 80%), mp 298.9-299.4 °C. ¹H NMR (400 MHz, DMSO-*d*₆): δ 10.13 (s, 1H), 10.09 (s, 1H), 8.85 (s, 1H), 8.04 (s, 1H), 7.74 (d, *J* = 8.0 Hz, 1H), 7.71 (s, 1H), 7.53 (t, *J* = 8.0 Hz, 1H), 7.31 (br, 2H), 7.07 (d, *J* = 8.0 Hz, 1H), 6.59 (br, 2H), 3.67 (s, 3H), 2.33 (q, *J* = 7.6 Hz, 2H), 1.07 (t, *J* = 7.6 Hz, 3H). HPLC purity: 98.1%, Retention time = 13.13 min. HRMS (ESI): exact mass calcd for C₂₂H₂₁N₆O₃ [M+H]⁺, 417.1675, found 417.1678.

4-(2-(4-methoxyphenylamino)-7-oxopteridin-8(7*H*)-yl)phenyl acrylate (3e): Red solid (yield 69%), mp 257.2-258.0 °C. ¹H NMR (400 MHz, DMSO-*d*₆): δ 10.15 (s, 1H), 8.87 (s, 1H), 8.06 (s, 1H), 7.51 (d, *J* = 8.8 Hz, 2H), 7.45 (d, *J* = 8.8 Hz, 2H), 7.31 (br, 2H), 6.69 (br, 2H), 6.60 (dd, *J* = 17.2, 1.6 Hz, 1H), 6.51 (dd, *J* = 17.2, 9.9 Hz, 1H), 6.22 (dd, *J* = 9.9, 1.6 Hz, 1H), 3.67 (s,

3H). HPLC purity: 97.8%, Retention time = 15.64 min. HRMS (ESI): exact mass calcd for $C_{22}H_{18}N_5O_4$ $[M+H]^+$, 416.1359, found 416.1359.

(E)-4-(dimethylamino)-N-(4-(2-(4-methoxyphenylamino)-7-oxopteridin-8(7H)-yl)phenyl)but-2-enamide (3f): Yellow solid (yield 55%), mp 273.5-274.3 °C. 1H NMR (400 MHz, DMSO- d_6): δ 10.45 (s, 1H), 10.10 (br, 1H), 8.85 (s, 1H), 8.05 (s, 1H), 7.87 (d, J = 8.8 Hz, 2H), 7.37 (d, J = 8.8 Hz, 2H), 7.30 (br, 2H), 6.82 (td, J = 15.4, 6.0 Hz, 1H), 6.60 (br, 2H), 6.40 (d, J = 15.4 Hz, 1H), 3.63 (s, 3H), 3.27 (d, J = 5.2 Hz, 2H), 2.33 (s, 6H). HPLC purity: 97.7%, Retention time = 10.47 min. HRMS (ESI): exact mass calcd for $C_{25}H_{26}N_7O_3$ $[M+H]^+$, 472.2097, found 472.2095.

(E)-4-(dimethylamino)-N-(3-(2-(4-methoxyphenylamino)-7-oxopteridin-8(7H)-yl)phenyl)but-2-enamide (3g): Yellow solid (yield 47%), mp 185.1-185.9 °C. 1H NMR (400 MHz, DMSO- d_6): δ 10.33 (s, 1H), 10.08 (br, 1H), 8.86 (s, 1H), 8.05 (s, 1H), 7.83 (d, J = 8.0 Hz, 1H), 7.78 (s, 1H), 7.55 (t, J = 8.0 Hz, 1H), 7.32 (br, 2H), 7.11 (d, J = 8.0 Hz, 1H), 6.74 (td, J = 15.2, 5.6 Hz, 1H), 6.59 (br, 2H), 6.30 (d, J = 15.2 Hz, 1H), 3.66 (s, 3H), 3.06 (d, J = 5.6 Hz, 2H), 2.17 (s, 6H). HPLC purity: 98.3%, Retention time = 10.74 min. HRMS (ESI): exact mass calcd for $C_{25}H_{24}N_7O_3$ $[M+H]^+$, 472.2097, found 472.2094.

(E)-4-(dimethylamino)-N-(4-(7-oxo-2-(phenylamino)pteridin-8(7H)-yl)phenyl)but-2-enamide (3h): Yellow solid (yield 53%), mp 225.3-226.1 °C. 1H NMR (400 MHz, DMSO- d_6): δ 10.37 (s, 1H), 10.19 (br, 1H), 8.90 (s, 1H), 8.08 (s, 1H), 7.87 (d, J = 8.4 Hz, 2H), 7.42 (d, J = 7.6 Hz, 2H), 7.38 (d, J = 8.4 Hz, 2H), 7.03 (br, 1H), 6.88 (t, J = 7.6 Hz, 1H), 6.82 (td, J = 15.4, 5.6 Hz, 1H), 6.37 (d, J = 15.4 Hz, 1H), 3.14 (d, J = 5.6 Hz, 2H), 2.24 (s, 6H). HPLC purity: 98.2%, Retention time = 10.55 min. HRMS (ESI): exact mass calcd for $C_{24}H_{24}N_7O_2$ $[M+H]^+$, 442.1991, found 442.1989.

(E)-4-(dimethylamino)-N-(3-(7-oxo-2-(phenylamino)pteridin-8(7H)-yl)phenyl)but-2-

enamide (3i): Yellow solid (yield 46%), mp 183.8-184.3 °C. ¹H NMR (400 MHz, DMSO-*d*₆): δ 10.32 (s, 1H), 10.17 (s, 1H), 8.90 (s, 1H), 8.08 (s, 1H), 7.81-7.79 (m, 2H), 7.55 (t, *J* = 8.0 Hz, 1H), 7.41 (d, *J* = 7.2 Hz, 2H), 7.12 (d, *J* = 8.0 Hz, 1H), 7.01 (br, 2H), 6.87 (t, *J* = 7.2 Hz, 1H), 6.73 (td, *J* = 15.2, 5.6 Hz, 1H), 6.28 (d, *J* = 15.2 Hz, 1H), 3.05 (d, *J* = 5.6 Hz, 2H), 2.16 (s, 6H). HPLC purity: 98.2%, Retention time = 10.85 min. HRMS (ESI): exact mass calcd for C₂₄H₂₄N₇O₂ [M+H]⁺, 442.1991, found 442.1996.

N-(4-(7-oxo-2-(phenylamino)pteridin-8(7H)-yl)phenyl)acrylamide (3j): Yellow solid (yield 79%), mp >300 °C. ¹H NMR (400 MHz, DMSO-*d*₆): δ 10.44 (s, 1H), 10.19 (br, 1H), 8.90 (s, 1H), 8.09 (s, 1H), 7.88 (d, *J* = 8.4 Hz, 2H), 7.41-7.38 (m, 4H), 7.03 (br, 2H), 6.88 (t, *J* = 7.2 Hz, 1H), 6.53 (dd, *J* = 16.8, 10.4 Hz, 1H), 6.35 (dd, *J* = 16.8, 1.6 Hz, 1H), 5.84 (dd, *J* = 10.4, 1.6 Hz, 1H). HPLC purity: 96.1%, Retention time = 12.68 min. HRMS (ESI): exact mass calcd for C₂₁H₁₇N₆O₂ [M+H]⁺, 385.1413, found 385.1405.

N-(3-(7-oxo-2-(phenylamino)pteridin-8(7H)-yl)phenyl)acrylamide (3k): Yellow solid (yield 74%), mp 270.1-270.9 °C. ¹H NMR (400 MHz, DMSO-*d*₆): δ 10.42 (s, 1H), 10.19 (s, 1H), 8.91 (s, 1H), 8.09 (s, 1H), 7.84-7.81 (m, 2H), 7.57 (t, *J* = 8.0 Hz, 1H), 7.41 (br, 2H), 7.15 (d, *J* = 7.6 Hz, 1H), 7.02 (br, 2H), 6.87 (t, *J* = 7.6 Hz, 1H), 6.45 (dd, *J* = 16.8, 10.4 Hz, 1H), 6.26 (dd, *J* = 16.8, 1.6 Hz, 1H), 5.77 (dd, *J* = 10.4, 1.6 Hz, 1H). HPLC purity: 96.8%, Retention time = 13.27 min. HRMS (ESI): exact mass calcd for C₂₁H₁₇N₆O₂ [M+H]⁺, 385.1413, found 385.1413.

N-(4-(2-(4-chlorophenylamino)-7-oxopteridin-8(7H)-yl)phenyl)acrylamide (3l): Yellow solid (yield 81%), mp >300 °C. ¹H NMR (400 MHz, DMSO-*d*₆): δ 10.46 (s, 1H), 10.34 (s, 1H), 8.92 (s, 1H), 8.11 (s, 1H), 7.88 (d, *J* = 8.8 Hz, 2H), 7.41-7.36 (m, 4H), 7.06 (br, 2H), 6.53 (dd, *J* = 16.8, 10.4 Hz, 1H), 6.36 (dd, *J* = 16.8, 1.6 Hz, 1H), 5.84 (dd, *J* = 10.4, 1.6 Hz, 1H). HPLC

purity: 94.3%, Retention time = 14.43 min. HRMS (ESI): exact mass calcd for $C_{21}H_{16}N_6O_2Cl$ $[M+H]^+$, 419.1023, found 419.1031.

***N*-(3-(2-(4-chlorophenylamino)-7-oxopteridin-8(7*H*)-yl)phenyl)acrylamide (3m):** Yellow solid (yield 78%), mp 259.1-259.8 °C. 1H NMR (400 MHz, DMSO- d_6): δ 10.44 (s, 1H), 10.34 (br, 1H), 8.93 (s, 1H), 8.11 (s, 1H), 7.84 (s, 1H), 7.81 (d, J = 8.4 Hz, 1H), 7.59 (t, J = 8.0 Hz, 1H), 7.43 (d, J = 7.2 Hz, 2H), 7.15 (d, J = 7.6 Hz, 1H), 6.46 (dd, J = 16.8, 10.4 Hz, 1H), 6.26 (dd, J = 16.8, 1.8 Hz, 1H), 5.77 (dd, J = 10.12, 1.8 Hz, 1H). HPLC purity: 97.4%, Retention time = 13.83 min. HRMS (ESI): exact mass calcd for $C_{21}H_{16}N_6O_2Cl$ $[M+H]^+$, 419.1023, found 419.1027.

***N*-(4-(2-(4-morpholinophenylamino)-7-oxopteridin-8(7*H*)-yl)phenyl)acrylamide (3n):** Red solid (yield 63%), mp >300 °C. 1H NMR (400 MHz, DMSO- d_6): δ 10.44 (s, 1H), 10.00 (s, 1H), 8.82 (s, 1H), 8.02 (s, 1H), 7.88 (d, J = 8.0 Hz, 1H), 7.36 (d, J = 8.4 Hz, 1H), 7.22 (br, 2H), 6.59 (br, 2H), 6.52 (dd, J = 17.2, 10.2 Hz, 1H), 6.33 (d, J = 17.2 Hz, 1H), 5.85 (d, J = 10.2 Hz, 1H), 3.67 (br, 4H), 2.92 (br, 4H). HPLC purity: 97.3%, Retention time = 12.21 min. HRMS (ESI): exact mass calcd for $C_{25}H_{24}N_7O_3$ $[M+H]^+$, 470.1941, found 470.1932.

***N*-(3-(2-(4-morpholinophenylamino)-7-oxopteridin-8(7*H*)-yl)phenyl)acrylamide (3o):** Red solid (yield 87%), mp >300 °C. 1H NMR (400 MHz, DMSO- d_6): δ 10.43 (s, 1H), 10.06 (s, 1H), 8.84 (s, 1H), 8.03 (s, 1H), 7.92 (br, 1H), 7.72 (s, 1H), 7.56 (t, J = 7.6 Hz, 1H), 7.27 (br, 2H), 7.12 (d, J = 7.2 Hz, 1H), 6.58 (br, 2H), 6.45 (dd, J = 16.8, 10.4 Hz, 1H), 6.26 (d, J = 16.8 Hz, 1H), 5.78 (d, J = 10.4 Hz, 1H), 3.71 (br, 4H), 2.94 (br, 4H). HPLC purity: 98.7%, Retention time = 11.71 min. HRMS (ESI): exact mass calcd for $C_{25}H_{24}N_7O_3$ $[M+H]^+$, 470.1941, found 470.1939.

***N*-(4-(2-(4-(4-methylpiperazin-1-yl)phenylamino)-7-oxopteridin-8(7*H*)-yl)phenyl)acrylamide (3p):** Red solid (yield 72%), mp 299.1-299.8 °C. 1H NMR (400 MHz,

DMSO-*d*₆): δ 10.51 (s, 1H), 10.06 (s, 1H), 8.83 (s, 1H), 8.03 (s, 1H), 7.89 (d, *J* = 8.4 Hz, 2H), 7.37 (d, *J* = 8.4 Hz, 2H), 7.17 (d, *J* = 6.4 Hz, 1H), 6.56-6.49 (m, 3H), 6.34 (d, *J* = 16.8 Hz, 1H), 5.85 (d, *J* = 10.8 Hz, 1H), 2.94 (br, 4H), 2.37 (br, 4H), 2.20 (s, 3H). HPLC purity: 97.0%, Retention time = 10.02 min. HRMS (ESI): exact mass calcd for C₂₆H₂₇N₈O₂ [M+H]⁺, 483.2257, found 483.2259.

***N*-(3-(2-(4-(4-methylpiperazin-1-yl)phenylamino)-7-oxopteridin-8(7*H*)-yl)phenyl)acrylamide (3q):** Red solid (yield 81%), mp 268.3-269.1 °C. ¹H NMR (400 MHz, DMSO-*d*₆): δ 10.45 (s, 1H), 10.06 (s, 1H), 8.84 (s, 1H), 8.04 (s, 1H), 7.93 (br, 1H), 7.73 (s, 1H), 7.56 (t, *J* = 8.0 Hz, 1H), 7.25 (br, 2H), 7.12 (d, *J* = 8.0 Hz, 1H), 6.57 (br, 2H), 6.46 (dd, *J* = 16.8, 10.4 Hz, 1H), 6.27 (dd, *J* = 16.8, 1.8 Hz, 1H), 5.78 (dd, *J* = 10.4, 1.8 Hz, 1H), 2.98 (br, 4H), 2.42 (br, 4H), 2.22 (s, 3H). HPLC purity: 96.5%, Retention time = 9.99 min. HRMS (ESI): exact mass calcd for C₂₆H₂₇N₈O₂ [M+H]⁺, 483.2257, found 483.2259.

***N*-(3-(7-oxo-2-(4-(piperidin-1-yl)phenylamino)pteridin-8(7*H*)-yl)phenyl)acrylamide (3r):** Red solid (yield 75%), mp 279.3-280.2 °C. ¹H NMR (400 MHz, DMSO-*d*₆): δ 10.44 (s, 1H), 10.03 (s, 1H), 8.83 (s, 1H), 8.02 (s, 1H), 7.94 (br, 1H), 7.73 (s, 1H), 7.55 (t, *J* = 8.0 Hz, 1H), 7.24 (br, 2H), 7.11 (d, *J* = 8.0 Hz, 1H), 6.57 (br, 2H), 6.46 (dd, *J* = 17.0, 10.2 Hz, 1H), 6.26 (dd, *J* = 17.0, 1.8 Hz, 1H), 5.77 (dd, *J* = 10.2, 1.8 Hz, 1H), 2.95 (br, 4H), 1.57 (br, 4H), 1.49 (br, 2H). HPLC purity: 95.3%, Retention time = 15.12 min. HRMS (ESI): exact mass calcd for C₂₆H₂₆N₇O₂ [M+H]⁺, 468.2148, found 468.2146.

***N*-(3-(7-oxo-2-(4-(pyrrolidin-1-yl)phenylamino)pteridin-8(7*H*)-yl)phenyl)acrylamide (3s):** Red solid (yield 77%), mp 279.5-280.1 °C. ¹H NMR (400 MHz, DMSO-*d*₆): δ 10.40 (s, 1H), 9.92 (s, 1H), 8.79 (s, 1H), 7.99 (s, 1H), 7.90 (br, 1H), 7.74 (br, 1H), 7.54 (t, *J* = 8.0 Hz, 1H), 7.20 (br, 2H), 7.10 (d, *J* = 8.0 Hz, 1H), 6.46 (dd, *J* = 17.0, 10.2 Hz, 1H), 6.26 (dd, *J* = 17.0, 1.8 Hz,

1H), 6.20 (br, 2H), 5.77 (dd, $J = 10.2, 1.8$ Hz, 1H), 3.10 (br, 4H), 1.91 (br, 4H). HPLC purity: 99.3%, Retention time = 15.12 min. HRMS (ESI): exact mass calcd for $C_{25}H_{24}N_7O_2$ $[M+H]^+$, 454.1991, found 454.1995.

***N*-(3-(2-(4-(diethylamino)phenylamino)-7-oxopteridin-8(7*H*)-yl)phenyl)acrylamide (3t):**
Red solid (yield 72%), mp 273.5-274.5 °C. 1H NMR (400 MHz, DMSO- d_6): δ 10.42 (s, 1H), 9.92 (s, 1H), 8.80 (s, 1H), 8.00 (s, 1H), 7.92 (br, 1H), 7.73 (s, 1H), 7.53 (t, $J = 8.0$ Hz, 1H), 7.19 (br, 2H), 7.09 (d, $J = 8.0$ Hz, 1H), 6.46 (dd, $J = 17.0, 10.2$ Hz, 1H), 6.32 (br, 2H), 6.27 (dd, $J = 17.0, 1.8$ Hz, 1H), 5.76 (dd, $J = 10.2, 1.8$ Hz, 1H), 3.20 (br, 4H), 1.00 (t, $J = 6.8$ Hz, 6H). HPLC purity: 96.2%, Retention time = 14.69 min. HRMS (ESI): exact mass calcd for $C_{25}H_{26}N_7O_2$ $[M+H]^+$, 456.2148, found 456.2143.

***N*-(3-(2-(4-acetamidophenylamino)-7-oxopteridin-8(7*H*)-yl)phenyl)acrylamide (3u):**
Yellow solid (yield 78%), mp 295.3-295.8 °C. 1H NMR (400 MHz, DMSO- d_6): δ 10.43 (s, 1H), 10.16 (br, 1H), 9.78 (s, 1H), 8.87 (s, 1H), 8.06 (s, 1H), 7.82 (d, $J = 8.0$ Hz, 1H), 7.79 (s, 1H), 7.56 (t, $J = 8.0$ Hz, 1H), 7.32 (br, 2H), 7.23 (br, 2H), 7.15 (d, $J = 8.0$ Hz, 1H), 6.46 (dd, $J = 17.0, 10.2$ Hz, 1H), 6.25 (dd, $J = 17.0, 1.8$ Hz, 1H), 5.76 (dd, $J = 10.2, 1.8$ Hz, 1H), 1.98 (s, 3H). HPLC purity: 95.4%, Retention time = 10.68 min. HRMS (ESI): exact mass calcd for $C_{23}H_{20}N_7O_3$ $[M+H]^+$, 442.1628, found 442.1624.

4-(8-(3-acrylamidophenyl)-7-oxo-7,8-dihydropteridin-2-ylamino)benzamide (3v): Yellow solid (yield 76%), mp 299.3-299.8 °C. 1H NMR (400 MHz, DMSO- d_6): δ 10.43 (s, 1H), 10.40 (s, 1H), 8.95 (s, 1H), 8.13 (s, 1H), 7.86 (s, 1H), 7.79 (d, $J = 8.0$ Hz, 1H), 7.71 (br, 1H), 7.61 (t, $J = 8.0$ Hz, 1H), 7.55 (d, $J = 7.6$ Hz, 2H), 7.47 (br, 2H), 7.18 (d, $J = 7.6$ Hz, 2H), 6.44 (dd, $J = 17.0, 10.2$ Hz, 1H), 6.25 (dd, $J = 17.0, 1.8$ Hz, 1H), 5.76 (dd, $J = 10.2, 1.8$ Hz, 1H). HPLC purity:

95.6%, Retention time = 10.00 min. HRMS (ESI): exact mass calcd for $C_{22}H_{18}N_7O_3$ $[M+H]^+$, 428.1471, found 428.1476.

***N*-(4-(2-(2-methoxy-4-(4-methylpiperazin-1-yl)phenylamino)-7-oxopteridin-8(7*H*)-yl)phenyl)acrylamide (3w):** Red solid (yield 71%), mp 265.4-266.2 °C. 1H NMR (400 MHz, DMSO- d_6): δ 10.43 (s, 1H), 8.80 (s, 1H), 8.42 (s, 1H), 8.03 (s, 1H), 7.85 (d, J = 8.6 Hz, 2H), 7.34 (d, J = 8.6 Hz, 2H), 7.25 (d, J = 8.8 Hz, 1H), 6.54-6.48 (m, 2H), 6.33 (dd, J = 17.0, 1.6 Hz, 1H), 6.02 (br, 1H), 5.84 (dd, J = 10.2, 1.6 Hz, 1H), 3.76 (s, 3H), 3.02 (br, 4H), 2.43 (br, 4H), 2.23 (s, 3H). HPLC purity: 97.1%, Retention time = 11.44 min. HRMS (ESI): exact mass calcd for $C_{27}H_{29}N_8O_3$ $[M+H]^+$, 513.2363, found 513.2362.

***N*-(3-(2-(2-methoxy-4-(4-methylpiperazin-1-yl)phenylamino)-7-oxopteridin-8(7*H*)-yl)phenyl)acrylamide (3x):** Red solid (yield 77%), mp 184.7-185.1 °C. 1H NMR (400 MHz, DMSO- d_6): δ 10.41 (s, 1H), 8.80 (s, 1H), 8.44 (br, 1H), 8.02 (s, 1H), 7.86 (br, 1H), 7.71 (s, 1H), 7.52 (t, J = 8.0 Hz, 1H), 7.30 (d, J = 7.6 Hz, 1H), 7.09 (d, J = 8.0 Hz, 1H), 6.53 (s, 1H), 6.46 (dd, J = 17.0, 10.2 Hz, 1H), 6.26 (dd, J = 17.0, 1.8 Hz, 1H), 6.02 (br, 1H), 5.78 (dd, J = 10.2, 1.8 Hz, 1H), 3.76 (s, 3H), 3.04 (br, 4H), 2.44 (br, 4H), 2.23 (s, 3H). HPLC purity: 96.2%, Retention time = 10.68 min. HRMS (ESI): exact mass calcd for $C_{27}H_{29}N_8O_3$ $[M+H]^+$, 513.2363, found 513.2361.

***N*-(4-(2-(4-methoxyphenylamino)-6-methyl-7-oxopteridin-8(7*H*)-yl)phenyl)acrylamide (3y):** Yellow solid (yield 78%), mp >300 °C. 1H NMR (400 MHz, DMSO- d_6): δ 10.44 (s, 1H), 9.90 (br, 1H), 8.77 (s, 1H), 7.87 (d, J = 8.8 Hz, 2H), 7.50 (d, J = 8.8 Hz, 2H), 7.29 (br, 2H), 6.59 (br, 2H), 6.52 (dd, J = 17.0, 10.0 Hz, 1H), 6.33 (dd, J = 17.0, 1.9 Hz, 1H), 5.82 (dd, J = 10.0, 1.9 Hz, 1H), 3.61 (s, 3H), 2.42 (s, 3H). HPLC purity: 95.9%, Retention time = 13.60 min. HRMS (ESI): exact mass calcd for $C_{23}H_{21}N_6O_3$ $[M+H]^+$, 429.1675, found 429.1671.

***N*-(3-(2-(4-methoxyphenylamino)-6-methyl-7-oxopteridin-8(7*H*)-yl)phenyl)acrylamide**

(3z): Yellow solid (yield 66%), mp 285.3-286.0 °C. ¹H NMR (400 MHz, DMSO-*d*₆): δ 10.42 (s, 1H), 9.93 (br, 1H), 8.78 (s, 1H), 7.83 (d, *J* = 8.0 Hz, 1H), 7.77 (s, 1H), 7.56 (t, *J* = 8.0 Hz, 1H), 7.31 (br, 2H), 7.11 (d, *J* = 8.0 Hz, 1H), 6.58 (br, 2H), 6.45 (dd, *J* = 17.0, 10.2 Hz, 1H), 6.26 (d, *J* = 17.0 Hz, 1H), 5.77 (d, *J* = 10.2 Hz, 1H), 3.65 (s, 3H), 2.42 (s, 3H). HPLC purity: 98.6%, Retention time = 13.51 min. HRMS (ESI): exact mass calcd for C₂₃H₂₁N₆O₃ [M+H]⁺, 429.1675, found 429.1675.

Cell Lines and Reagents.⁴⁵ The H1975 (NSCLC, EGFR-T790M/L858R) and HCC827 (NSCLC, EGFR-delE746_A750) cells were obtained from ATCC. The cells were maintained at 37 °C in a 5% CO₂ incubator in RPMI 1640 medium (Gibco, Invitrogen) containing 10% fetal bovine serum (Gibco, Invitrogen). The EGFR gene for each cell line was sequenced prior to use. Gefitinib was synthesized in the laboratory of Dr. Ke Ding.

In Vitro Enzymatic Activity Assay.⁴⁵ Wild-type and different EGFR mutants (L858R, T790M/L858R) and the Z'-Lyte Kinase Assay Kit were purchased from Invitrogen™. Concentration gradients consisting of 10 levels from 5.1 × 10⁻¹¹ to 1.0 × 10⁻⁶ mol/L were used for all the tested compounds. The experiments were performed according to the manufacturer instructions.

Kinase Profiling Study. The kinase profiling study was conducted using the KINOMEscan platform (www.discoverx.com). The detailed protocol description is provided in the Supporting Information.

Cell Proliferation and Growth Inhibition Assay.⁴⁵ The cell proliferation was assessed using the MTS assay. The cells were exposed to the treatment for 72 h, and the number of cells used per experiment for each cell line was adjusted to obtain an absorbance between 1.3 and 2.2 at

490 nm. Six concentrations (0.1 nM to 10 μ M) of each compound were tested. At least six replicates of each concentration were used. All experiments were repeated at least four times. The data were analyzed using GraphPad Prism version 4.0 to determine the IC₅₀, which were fitted using a nonlinear regression model with a sigmoidal dose-response.

Mouse Tumor Xenograft Efficacy Study. The efficacy study was conducted as previously reported,⁴⁵ in accordance with the guidelines for the Care and Use of Laboratory Animals in Guangzhou Institute of Biomedicine and Health (GIBH, CAS). Six week old SCID mice were inoculated subcutaneously with H1975 NSCLC cells (2×10^6 /mouse) in the right flank. Upon reaching an average tumor volume of 480–540 mm³ (14 days post implantation), animals were randomized into treatment groups (n = 6 mice/group). Each group was treated via dosed IP injection for 14 days with either vehicle only or with compound **3x** at 20 or 40 mg/kg daily (qd). The doses were in a volume of 0.1 mL/10 g of the animal body weight. Tumor volumes were measured every other day using vernier calipers, and volumes were calculated using the following formula: tumor volume (mm³) = $W^2(L/2)$, where W = width and L = length in mm.

ASSOCIATED CONTENT

Supporting Information. Full experimental details, including enzymatic activity assay, kinase profiling, tumor cellular activity assay, and top 100 compound hits identified by SHAFTS. This material is available free of charge via the Internet at <http://pubs.acs.org>.

AUTHOR INFORMATION

Corresponding Author

Email: hlli@ecust.edu.cn, yfxu@ecust.edu.cn, ding_ke@gibh.ac.cn

1
2
3
4
5
6
7
8
9
10
11
12
13
14
15
16
17
18
19
20
21
22
23
24
25
26
27
28
29
30
31
32
33
34
35
36
37
38
39
40
41
42
43
44
45
46
47
48
49
50
51
52
53
54
55
56
57
58
59
60

Author Contributions

‡These authors contributed equally.

Notes

The authors declare no competing financial interest.

ACKNOWLEDGMENT

The research is supported in part by the Fundamental Research Funds for the Central Universities, the National Natural Science Foundation of China (grants 81222046, 21173076, 81102375, 21302054, 21236002 and 81230076), the Special Fund for Major State Basic Research Project (grant 2009CB918501), the Shanghai Committee of Science and Technology (grants 11DZ2260600 and 12401900801), and the 863 Hi-Tech Program of China (grant 2012AA020308). Honglin Li is also sponsored by Program for New Century Excellent Talents in University (grant NCET-10-0378) and Shanghai Rising-Star Tracking Program (grant 13QH1401100).

REFERENCES

- (1) Ciardello, F.; Tortora, G. EGFR Antagonists in Cancer Treatment. *N. Engl. J. Med.* **2008**, 358, 1160-1174.
- (2) Olayioye, M. A.; Neve, R. M.; Lane, H. A.; Hynes, N. E. The ErbB signaling network: receptor heterodimerization in development and cancer. *EMBO J.* **2000**, 19, 3159-3167.
- (3) Sharma, S. V.; Bell, D. W.; Settleman, J.; Haber, D. A. Epidermal growth factor receptor mutations in lung cancer. *Nat. Rev. Cancer.* **2007**, 7, 169-181.
- (4) Wu, C. H.; Coumar, M. S.; Chu, C. Y.; Lin, W. H.; Chen, Y. R.; Chen, C. T.; Shiao, H. Y.; Rafi, S.; Wang, S. Y.; Hsu, H.; Chen, C. H.; Chang, C. Y.; Chang, T. Y.; Lien, T. W.; Fang, M. Y.; Yeh, K. C.; Chen, C. P.; Yeh, T. K.; Hsieh, S. H.; Hsu, J. T.; Liao, C. C.; Chao, Y. S.; Hsieh, H. P. Design and synthesis of tetrahydropyridothieno[2,3-d]pyrimidine scaffold based epidermal growth factor receptor (EGFR) kinase inhibitors: the role of side chain chirality and Michael acceptor group for maximal potency. *J. Med. Chem.* **2010**, 53, 7316-7326.
- (5) Janku, F.; Stewart, D. J.; Kurzrock, R. Targeted therapy in non-small-cell lung cancer[mdash]is it becoming a reality? *Nat. Rev. Clin. Oncol.* **2011**, 8, 384-384.
- (6) Rosell, R.; Moran, T.; Queralt, C.; Porta, R.; Cardenal, F.; Camps, C.; Majem, M.; Lopez-Vivanco, G.; Isla, D.; Provencio, M.; Insa, A.; Massuti, B.; Gonzalez-Larriba, J. L.; Paz-Ares, L.; Bover, I.; Garcia-Campelo, R.; Moreno, M. A.; Catot, S.; Rolfo, C.; Reguart, N.; Palmero, R.; Sánchez, J. M.; Bastus, R.; Mayo, C.; Bertran-Alamillo, J.; Molina, M. A.; Sanchez, J. J.; Taron, M. Screening for Epidermal Growth Factor Receptor Mutations in Lung Cancer. *N. Engl. J. Med.* **2009**, 361, 958-967.

(7) Carey, K. D.; Garton, A. J.; Romero, M. S.; Kahler, J.; Thomson, S.; Ross, S.; Park, F.; Haley, J. D.; Gibson, N.; Sliwkowski, M. X. Kinetic Analysis of Epidermal Growth Factor Receptor Somatic Mutant Proteins Shows Increased Sensitivity to the Epidermal Growth Factor Receptor Tyrosine Kinase Inhibitor, Erlotinib. *Cancer Res.* **2006**, 66, 8163-8171.

(8) Yun, C.-H.; Boggon, T. J.; Li, Y.; Woo, M. S.; Greulich, H.; Meyerson, M.; Eck, M. J. Structures of Lung Cancer-Derived EGFR Mutants and Inhibitor Complexes: Mechanism of Activation and Insights into Differential Inhibitor Sensitivity. *Cancer Cell* **2007**, 11, 217-227.

(9) Oxnard, G. R.; Arcila, M. E.; Chmielecki, J.; Ladanyi, M.; Miller, V. A.; Pao, W. New Strategies in Overcoming Acquired Resistance to Epidermal Growth Factor Receptor Tyrosine Kinase Inhibitors in Lung Cancer. *Clin. Cancer. Res.* **2011**, 17, 5530-5537.

(10) Pallis, A.; Briasoulis, E.; Linardou, H.; Papadimitriou, C.; Bafaloukos, D.; Kosmidis, P.; Murray, S. Mechanisms of resistance to epidermal growth factor receptor tyrosine kinase inhibitors in patients with advanced non-small-cell lung cancer: clinical and molecular considerations. *Curr. Med. Chem.* **2011**, 18, 1613-1628.

(11) Carmi, C.; Lodola, A.; Rivara, S.; Vacondio, F.; Cavazzoni, A.; Alfieri, R. R.; Ardizzoni, A.; Petronini, P. G.; Mor, M. Epidermal Growth Factor Receptor Irreversible Inhibitors: Chemical Exploration of the Cysteine-Trap Portion. *Mini. Rev. Med. Chem.* **2011**, 11, 1019-1030.

(12) Ercan, D.; Zejnullahu, K.; Yonesaka, K.; Xiao, Y.; Capelletti, M.; Rogers, A.; Lifshits, E.; Brown, A.; Lee, C.; Christensen, J. G.; Kwiatkowski, D. J.; Engelman, J. A.; Janne, P. A. Amplification of EGFR T790M causes resistance to an irreversible EGFR inhibitor. *Oncogene* **2010**, 29, 2346-2356.

(13) Gazdar, A. F. Activating and resistance mutations of EGFR in non-small-cell lung cancer: role in clinical response to EGFR tyrosine kinase inhibitors. *Oncogene* **2009**, 28, S24-S31.

(14) Yun, C. H.; Mengwasser, K. E.; Toms, A. V.; Woo, M. S.; Greulich, H.; Wong, K. K.; Meyerson, M.; Eck, M. J. The T790M mutation in EGFR kinase causes drug resistance by increasing the affinity for ATP. *Proc. Natl. Acad. Sci. U.S.A.* **2008**, 105, 2070-2075.

(15) Zhou, W.; Ercan, D.; Chen, L.; Yun, C. H.; Li, D.; Capelletti, M.; Cortot, A. B.; Chirieac, L.; Iacob, R. E.; Padera, R.; Engen, J. R.; Wong, K. K.; Eck, M. J.; Gray, N. S.; Janne, P. A. Novel mutant-selective EGFR kinase inhibitors against EGFR T790M. *Nature* **2009**, 462, 1070-1074.

(16) Smaill, J. B.; Showalter, H. D. H.; Zhou, H.; Bridges, A. J.; McNamara, D. J.; Fry, D. W.; Nelson, J. M.; Sherwood, V.; Vincent, P. W.; Roberts, B. J.; Elliott, W. L.; Denny, W. A. Tyrosine Kinase Inhibitors. 18. 6-Substituted 4-Anilinoquinazolines and 4-Anilinopyrido[3,4-d]pyrimidines as Soluble, Irreversible Inhibitors of the Epidermal Growth Factor Receptor. *J. Med. Chem.* **2001**, 44, 429-440.

(17) Kwak, E. L.; Sordella, R.; Bell, D. W.; Godin-Heymann, N.; Okimoto, R. A.; Brannigan, B. W.; Harris, P. L.; Driscoll, D. R.; Fidias, P.; Lynch, T. J.; Rabindran, S. K.; McGinnis, J. P.; Wissner, A.; Sharma, S. V.; Isselbacher, K. J.; Settleman, J.; Haber, D. A. Irreversible inhibitors of the EGF receptor may circumvent acquired resistance to gefitinib. *Proc. Natl. Acad. Sci. U.S.A.* **2005**, 102, 7665-7670.

(18) Li, D.; Ambrogio, L.; Shimamura, T.; Kubo, S.; Takahashi, M.; Chirieac, L. R.; Padera, R. F.; Shapiro, G. I.; Baum, A.; Himmelsbach, F.; Rettig, W. J.; Meyerson, M.; Solca, F.;

Greulich, H.; Wong, K. K. BIBW2992, an irreversible EGFR/HER2 inhibitor highly effective in preclinical lung cancer models. *Oncogene* **2008**, 27, 4702-4711.

(19) Tsou, H.-R.; Overbeek-Klumpers, E. G.; Hallett, W. A.; Reich, M. F.; Floyd, M. B.; Johnson, B. D.; Michalak, R. S.; Nilakantan, R.; Discafani, C.; Golas, J.; Rabindran, S. K.; Shen, R.; Shi, X.; Wang, Y.-F.; Upeslakis, J.; Wissner, A. Optimization of 6,7-Disubstituted-4-(arylamino)quinoline-3-carbonitriles as Orally Active, Irreversible Inhibitors of Human Epidermal Growth Factor Receptor-2 Kinase Activity. *J. Med. Chem.* **2005**, 48, 1107-1131.

(20) Engelman, J. A.; Zejnullahu, K.; Gale, C.-M.; Lifshits, E.; Gonzales, A. J.; Shimamura, T.; Zhao, F.; Vincent, P. W.; Naumov, G. N.; Bradner, J. E.; Althaus, I. W.; Gandhi, L.; Shapiro, G. I.; Nelson, J. M.; Heymach, J. V.; Meyerson, M.; Wong, K.-K.; Jänne, P. A. PF00299804, an Irreversible Pan-ERBB Inhibitor, Is Effective in Lung Cancer Models with EGFR and ERBB2 Mutations that Are Resistant to Gefitinib. *Cancer Res.* **2007**, 67, 11924-11932.

(21) Fry, D. W.; Bridges, A. J.; Denny, W. A.; Doherty, A.; Greis, K. D.; Hicks, J. L.; Hook, K. E.; Keller, P. R.; Leopold, W. R.; Loo, J. A.; McNamara, D. J.; Nelson, J. M.; Sherwood, V.; Smaill, J. B.; Trumpp-Kallmeyer, S.; Dobrusin, E. M. Specific, irreversible inactivation of the epidermal growth factor receptor and erbB2, by a new class of tyrosine kinase inhibitor. *Proc. Natl. Acad. Sci. U.S.A.* **1998**, 95, 12022-12027.

(22) Blair, J. A.; Rauh, D.; Kung, C.; Yun, C.-H.; Fan, Q.-W.; Rode, H.; Zhang, C.; Eck, M. J.; Weiss, W. A.; Shokat, K. M. Structure-guided development of affinity probes for tyrosine kinases using chemical genetics. *Nat. Chem. Biol.* **2007**, 3, 229-238.

- (23) Leproult, E.; Barluenga, S.; Moras, D.; Wurtz, J.-M.; Winssinger, N. Cysteine Mapping in Conformationally Distinct Kinase Nucleotide Binding Sites: Application to the Design of Selective Covalent Inhibitors. *J. Med. Chem.* **2011**, 54, 1347-1355.
- (24) Singh, J.; Petter, R. C.; Kluge, A. F. Targeted covalent drugs of the kinase family. *Curr. Opin. Chem. Biol.* **2010**, 14, 475-480.
- (25) Karikios, D. J.; Boyer, M. J. Irreversible EGFR inhibitors in advanced non-small-cell lung carcinoma: rationale and clinical evidence. *Clinical Investigation* **2012**, 2, 317-325.
- (26) Ou, S.-H. I. Second-generation irreversible epidermal growth factor receptor (EGFR) tyrosine kinase inhibitors (TKIs): A better mousetrap? A review of the clinical evidence. *Crit. Rev. Oncol./Hematol.* **2012**, 83, 407-421.
- (27) Bai, F.; Liu, H.; Tong, L.; Zhou, W.; Liu, L.; Zhao, Z.; Liu, X.; Jiang, H.; Wang, X.; Xie, H.; Li, H. Discovery of novel selective inhibitors for EGFR-T790M/L858R. *Bioorg. Med. Chem. Lett.* **2012**, 22, 1365-1370.
- (28) Gray, N. S.; Janne, P.; Eck, M. J. EGFR Inhibitors and Methods of Treating Disorders. WO2010129053A2, Nov 11, 2010.
- (29) Bergmann, R.; Linusson, A.; Zamora, I. SHOP: Scaffold HOPping by GRID-Based Similarity Searches. *J. Med. Chem.* **2007**, 50, 2708-2717.
- (30) Lloyd, D. G.; Buenemann, C. L.; Todorov, N. P.; Manallack, D. T.; Dean, P. M. Scaffold Hopping in De Novo Design. Ligand Generation in the Absence of Receptor Information. *J. Med. Chem.* **2004**, 47, 493-496.

- (31) Jenkins, J. L.; Glick, M.; Davies, J. W. A 3D Similarity Method for Scaffold Hopping from Known Drugs or Natural Ligands to New Chemotypes. *J. Med. Chem.* **2004**, 47, 6144-6159.
- (32) Barker, E. J.; Buttar, D.; Cosgrove, D. A.; Gardiner, E. J.; Kitts, P.; Willett, P.; Gillet, V. J. Scaffold Hopping Using Clique Detection Applied to Reduced Graphs. *J. Chem. Inf. Model.* **2006**, 46, 503-511.
- (33) Wale, N.; Watson, I. A.; Karypis, G. Indirect Similarity Based Methods for Effective Scaffold-Hopping in Chemical Compounds. *J. Chem. Inf. Model.* **2008**, 48, 730-741.
- (34) Stiefl, N.; Watson, I. A.; Baumann, K.; Zaliani, A. ErG:□ 2D Pharmacophore Descriptions for Scaffold Hopping. *J. Chem. Inf. Model.* **2006**, 46, 208-220.
- (35) Sperandio, O.; Andrieu, O.; Miteva, M. A.; Vo, M.-Q.; Souaille, M.; Delfaud, F.; Villoutreix, B. O. MED-SuMoLig:□ A New Ligand-Based Screening Tool for Efficient Scaffold Hopping. *J. Chem. Inf. Model.* **2007**, 47, 1097-1110.
- (36) Rush, T. S.; Grant, J. A.; Mosyak, L.; Nicholls, A. A Shape-Based 3-D Scaffold Hopping Method and Its Application to a Bacterial Protein–Protein Interaction. *J. Med. Chem.* **2005**, 48, 1489-1495.
- (37) Maass, P.; Schulz-Gasch, T.; Stahl, M.; Rarey, M. Recore:□ A Fast and Versatile Method for Scaffold Hopping Based on Small Molecule Crystal Structure Conformations. *J. Chem. Inf. Model.* **2007**, 47, 390-399.

(38) Liu, X.; Jiang, H.; Li, H. SHAFTS: A Hybrid Approach for 3D Molecular Similarity Calculation. 1. Method and Assessment of Virtual Screening. *J. Chem. Inf. Model.* **2011**, 51, 2372-2385.

(39) Nicholls, A.; McGaughey, G. B.; Sheridan, R. P.; Good, A. C.; Warren, G.; Mathieu, M.; Muchmore, S. W.; Brown, S. P.; Grant, J. A.; Haigh, J. A.; Nevins, N.; Jain, A. N.; Kelley, B. Molecular Shape and Medicinal Chemistry: A Perspective. *J. Med. Chem.* **2010**, 53, 3862-3886.

(40) Lu, W.; Liu, X.; Cao, X.; Xue, M.; Liu, K.; Zhao, Z.; Shen, X.; Jiang, H.; Xu, Y.; Huang, J.; Li, H. SHAFTS: A Hybrid Approach for 3D Molecular Similarity Calculation. 2. Prospective Case Study in the Discovery of Diverse p90 Ribosomal S6 Protein Kinase 2 Inhibitors To Suppress Cell Migration. *J. Med. Chem.* **2011**, 54, 3564-3574.

(41) Voigt, J. H.; Bienfait, B.; Wang, S.; Nicklaus, M. C. Comparison of the NCI Open Database with Seven Large Chemical Structural Databases. *J. Chem. Inf. Comput. Sci.* **2001**, 41, 702-712.

(42) Gong, J.; Cai, C.; Liu, X.; Ku, X.; Jiang, H.; Gao, D.; Li, H. ChemMapper: a versatile web server for exploring pharmacology and chemical structure association based on molecular 3D similarity method. *Bioinformatics* **2013**, 29, 1827-1829.

(43) NSC86929 - Compound Summary.
<http://pubchem.ncbi.nlm.nih.gov/summary/summary.cgi?cid=258174#x299> (April 2, 2012).

(44) Tsou, H.-R.; Mamuya, N.; Johnson, B. D.; Reich, M. F.; Gruber, B. C.; Ye, F.; Nilakantan, R.; Shen, R.; Discafani, C.; DeBlanc, R.; Davis, R.; Koehn, F. E.; Greenberger, L. M.; Wang, Y.-F.; Wissner, A. 6-Substituted-4-(3-bromophenylamino)quinazolines as Putative

Irreversible Inhibitors of the Epidermal Growth Factor Receptor (EGFR) and Human Epidermal Growth Factor Receptor (HER-2) Tyrosine Kinases with Enhanced Antitumor Activity. *J. Med. Chem.* **2001**, 44, 2719-2734.

(45) Chang, S.; Zhang, L.; Xu, S.; Luo, J.; Lu, X.; Zhang, Z.; Xu, T.; Liu, Y.; Tu, Z.; Xu, Y.; Ren, X.; Geng, M.; Ding, J.; Pei, D.; Ding, K. Design, Synthesis, and Biological Evaluation of Novel Conformationally Constrained Inhibitors Targeting Epidermal Growth Factor Receptor Threonine790 → Methionine790 Mutant. *J. Med. Chem.* **2012**, 55, 2711-2723.

(46) Zhou, W.; Ercan, D.; Jänne, P. A.; Gray, N. S. Discovery of selective irreversible inhibitors for EGFR-T790M. *Bioorg. Med. Chem. Lett.* **2011**, 21, 638-643.

(47) Xu, S.; Zhang, L.; Chang, S.; Luo, J.; Lu, X.; Tu, Z.; Liu, Y.; zhang, Z.; Xu, Y.; Ren, X.; Ding, K. Design, synthesis and biological evaluation of new molecules inhibiting epidermal growth factor receptor threonine790 → methionine790 mutant. *MedChemComm* **2012**, 3, 1155-1159.

(48) Xu, T.; Zhang, L.; Xu, S.; Yang, C.-Y.; Luo, J.; Ding, F.; Lu, X.; Liu, Y.; Tu, Z.; Li, S.; Pei, D.; Cai, Q.; Li, H.; Ren, X.; Wang, S.; Ding, K. Pyrimido[4,5-d]pyrimidin-4(1H)-one Derivatives as Selective Inhibitors of EGFR Threonine790 to Methionine790 (T790M) Mutants. *Angewandte Chemie International Edition* **2013**, 52, 8387-8390.

(49) Fabian, M. A.; Biggs, W. H.; Treiber, D. K.; Atteridge, C. E.; Azimioara, M. D.; Benedetti, M. G.; Carter, T. A.; Ciceri, P.; Edeen, P. T.; Floyd, M.; Ford, J. M.; Galvin, M.; Gerlach, J. L.; Grotzfeld, R. M.; Herrgard, S.; Insko, D. E.; Insko, M. A.; Lai, A. G.; Lelias, J.-M.; Mehta, S. A.; Milanov, Z. V.; Velasco, A. M.; Wodicka, L. M.; Patel, H. K.; Zarrinkar, P. P.;

1
2
3 Lockhart, D. J. A small molecule-kinase interaction map for clinical kinase inhibitors. *Nat*
4
5 *Biotech* **2005**, 23, 329-336.
6
7

8
9 (50) ChemMapper Server. <http://lilab.ecust.edu.cn/chemmapper/> (April 1, 2012).
10

11 (51) Liu, X.; Bai, F.; Ouyang, S.; Wang, X.; Li, H.; Jiang, H. Cyndi: a multi-objective
12 evolution algorithm based method for bioactive molecular conformational generation. *BMC*
13 *Bioinformatics* **2009**, 10, 101.
14
15
16
17

18
19 (52) Liu, K. K. C.; Bagrodia, S.; Bailey, S.; Cheng, H.; Chen, H.; Gao, L.; Greasley, S.;
20 Hoffman, J. E.; Hu, Q.; Johnson, T. O.; Knighton, D.; Liu, Z.; Marx, M. A.; Nambu, M. D.;
21 Ninkovic, S.; Pascual, B.; Rafidi, K.; Rodgers, C. M. L.; Smith, G. L.; Sun, S.; Wang, H.; Yang,
22 A.; Yuan, J.; Zou, A. 4-Methylpteridinones as orally active and selective PI3K/mTOR dual
23
24
25
26
27
28
29
30
31
32
33
34
35
36
37
38
39
40
41
42
43
44
45
46
47
48
49
50
51
52
53
54
55
56
57
58
59
60 inhibitors. *Bioorg. Med. Chem. Lett.* **2010**, 20, 6096-6099.

Table of Contents Graphic

